

# Properties of Luminous Red Galaxies in the Sloan Digital Sky Survey

Tom Barber<sup>1\*</sup>, Avery Meiksin<sup>1\*</sup> and Tara Murphy<sup>2\*</sup>

<sup>1</sup> *SUPA†; Institute for Astronomy, University of Edinburgh, Royal Observatory, Edinburgh, EH9 3HJ*

<sup>2</sup> *School of Physics and School of Information Technologies, University of Sydney, NSW 2006, Australia*

8 June 2021

## ABSTRACT

We perform population synthesis modelling of a magnitude-limited sample of 4391 Luminous Red Galaxies selected from the Sloan Digital Sky Survey Data Release 4 (SDSS DR4). We fit measured spectral indices using a large library of high resolution spectra, covering a wide range of metallicities and assuming an exponentially decaying star-formation rate punctuated by bursts, to obtain median-likelihood estimates for the light-weighted age, metallicity, stellar mass and extinction for the galaxies. The ages lie predominantly in the range 4–10 Gyr, peaking near 6 Gyr, with metallicities in the range  $-0.4 < [Z/H] < 0.4$ , peaking at  $[Z/H] \approx 0.2$ . Only a few per cent of the spectra are better fit allowing for a burst in addition to continuous star-formation. For these systems, typically one-quarter to one-third of the stars are formed in the burst. The total stellar masses of all the galaxies are confined to a very narrow range around  $\sim 3 \times 10^{11} M_{\odot}$ , consistent with the expected homogeneity of the sample. Our results broadly agree with those of previous groups using an independent population synthesis code. We find, however, that our choice in priors results in ages 1–2 Gyr smaller, decreasing the peak formation epoch from about  $z = 2.3$  to  $z = 1.3$  for the stars. To describe the distribution in measured mean metallicity of the galaxies, we develop a metal evolution model incorporating stochastic star-formation quenching motivated by recent attempts to account for the apparent ‘anti-hierarchical’ formation of elliptical galaxies. Two scenarios emerge, a closed box with an effective stellar yield of 0.26, and an accreting box with an effective stellar yield of 0.10. Both scenarios require an IMF weighted towards massive stars. They also require characteristic star-formation quenching times of about  $10^8$  yr, the expected lifetime of luminous Quasi-Stellar Objects. The models predict an anti-correlation between the age and mean metallicity of the galaxies similar to that observed.

**Key words:** galaxies: elliptical and lenticular, cD - galaxies: evolution - galaxies: formation - galaxies: fundamental parameters - galaxies: stellar content

## 1 INTRODUCTION

In the hierarchical merger scenario of structure formation, more massive systems form from the merger of less massive ones (Peebles & Dicke 1968; Peebles 1983). While numerical simulations of the evolution of dark matter haloes in a Cold Dark Matter dominated universe bear this out (Davis et al. 1985), predictions in the hierarchical scenario for galaxies are complicated by the need to account for gaseous dissipation (White & Rees 1978), without which galaxies would lose their integrity at each level of the merger hierarchy.

The most straightforward prediction of the hierarchical scenario is that smaller mass galaxies form prior to the more massive, although the effects of galaxy mergers, as distinct from halo mergers, could substantially complicate this picture (Blumenthal et al. 1984). Early semi-analytic estimates of the formation and properties of galaxies have suggested that half of the stars in the Universe formed at redshifts  $z < 1.5$ , and only some 10 per cent at  $z > 3$  (Cole et al. 1994; Baugh et al. 1998). Elliptical galaxies in particular are predicted to show a trend of decreasing age with increasing luminosity, with the brightest ellipticals the youngest (Kauffmann 1996; Kauffmann & Charlot 1998).

Observations have generally not supported the predicted ages and their trends with galaxy properties. The contrary evidence is derived primarily from two methods:

\* E-mail: tjb@roe.ac.uk (TJB); aam@roe.ac.uk (AM); tara@physics.usyd.edu.au (TM)

† Scottish Universities Physics Alliance

measurements of the luminosity function of galaxies and its evolution, and age estimates based on population synthesis. Cowie et al. (1996) discovered that the characteristic luminosity of galaxies undergoing rapid star formation has been declining with time at redshifts  $z < 1.7$ , a result extended to  $z \approx 3$  by Sawicki et al. (1997). As a function of galaxy class, the later the type of galaxy, the later is its peak period of star formation (Heyl et al. 1997). Since then, an abundance of evidence for anti-hierarchical galaxy formation (or so-called ‘downsizing’) has accrued based on galaxy number counts and colours, generally indicating that the ‘quenching mass’, at which the major episode of star formation ceases, decreases with decreasing redshift (Pozzetti et al. 2003; Fontana et al. 2004; Bundy et al. 2005; Drory et al. 2005; Bundy et al. 2005; Cimatti et al. 2006). Massive galaxies appear to undergo a higher merger rate at high redshifts ( $z \approx 3$ ) than at low redshifts, settling down by  $z \approx 1.5$  (Conselice 2006), again in apparent opposition to the hierarchical merger scenario.

The picture that appears to be developing is that star formation occurred early in systems with a wide range of masses, but was terminated through some unknown process, first in the progenitors of the most massive galaxies, and progressing steadily towards less massive systems with time. The progenitors of massive galaxies (with stellar masses today in excess of  $10^{10} M_{\odot}$ ), subsequently merged, possibly with a small amount of additional star formation, but settled into largely quiescent systems by  $z = 1.5$ .

Numerical modellers have sought to catch up with these findings, drawing increasingly on the role of feedback. While supernova feedback has long been assigned a key role in regulating star formation, Active Galactic Nuclei have now been invoked as a means of terminating star formation in the most massive systems, and proposed as the origin of the dichotomy between blue galaxies and the more massive red (Dekel & Birnboim 2006). Incorporating feedback by supernovae and Active Galactic Nuclei has become a promising means of reconciling the mass-sensitive evolution in number counts, the merger rates, and the ages of stellar populations (Bower et al. 2006; Lucia & Blaizot 2006). These models may be expected to develop further as knowledge of the star formation history of galaxies of different masses and in different environments continues to grow increasingly precise.

In the past, population synthesis model estimates of ages were long plagued by the age-metallicity degeneracy. Improvements in the stellar atmosphere models, the data, and the understanding of the sensitivity of absorption lines to age and metallicity have since led to more reliable age and metallicity determinations. Trager et al. (2000b,a) found a range of ages for elliptical galaxies in the field, with lower velocity-dispersion galaxies tending to be younger. By contrast, ellipticals in clusters tend to be old. They also found that larger velocity-dispersion galaxies tend to show increased suppression of iron-peak elements. Caldwell et al. (2003) similarly found that smaller velocity dispersion systems tend to have younger luminosity-weighted ages. Evidence for recent burst activity in field ellipticals was found by Treu et al. (2002). Thomas et al. (2005) have suggested a shift in the peak star formation epochs of early type galaxies, with massive early-type galaxies in low-density environments  $\sim 2$  Gyr younger than their high-density environment

counterparts, and the star formation rate peak shifting to lower redshifts the lower the mass of the galaxy. Old ages for cluster ellipticals were similarly found by Yamada et al. (2006).

Estimates of the current to mean star formation rates, or ‘birthrate,’ of galaxies using population synthesis models for galaxies of a range in mass and type show a trend of decreasing birthrate with increasing stellar mass (Boselli et al. 2001; Gavazzi et al. 2002; Kauffmann et al. 2003; Brinchmann et al. 2004; Gallazzi et al. 2005), again indicating that the more massive a galaxy is, the earlier most of its stars were formed.

The confluence of wide-field surveys and high-speed computing is now making feasible the testing of galaxy formation scenarios by detailed population synthesis models with a spectral resolution and coverage previously impossible on a large scale. In this paper, we apply population synthesis models to estimate the mass, metallicities, and star formation histories of Luminous Red Galaxies (LRGs) drawn from the Sloan Digital Sky Survey (SDSS) (York & et al. 2000). We have several reasons for concentrating on LRGs: 1. they form a large sample of galaxies chosen according to well-defined selection criteria forming a well-defined sample (Eisenstein & et al. 2001), 2. the galaxies form a uniform population both photometrically (Faber 1973; Visvanathan & Sandage 1977), and spectroscopically (Faber 1973; Eisenstein & et al. 2003), 3. the galaxies are bright, providing high signal-to-noise ratio spectra, 4. they represent the extreme high mass end of galaxy stellar masses and an extreme in anti-hierarchical behaviour, 5. star formation has ceased in all but a few percent of the systems (Roseboom & et al. 2006), and so the influence of emission lines associated with ongoing star formation on the key absorption features used to infer the properties of the galaxies is minimal, 6. they are an intrinsically interesting class of objects, being the most massive and most strongly clustered galaxies in the Universe.

Population synthesis analyses for galaxies in SDSS Data Release 2 (DR2) and earlier data were performed previously by Kauffmann et al. (2003) (hereafter K03), Brinchmann et al. (2004) and Gallazzi et al. (2005) (hereafter G05). These studies provide useful comparisons for our results. Our analysis, however, differs in several respects from these earlier efforts. We exploit high resolution synthetic spectra to model several absorption indices that match the resolution of the spectra. The analyses of K03 and Brinchmann et al. (2004) used the 4000-Å break ( $D_n4000$ ) and Balmer absorption, or emission lines, to estimate the star formation rates and histories. The closest population synthesis analysis to ours is that of G05, who similarly based their model-fitting on several high resolution absorption features. This work, however, differs from theirs as follows: 1. an alternative population synthesis model is used, utilising an independent set of stellar templates to construct the spectra and a different set of stellar evolution tracks, 2. the sample of LRGs analysed is substantially larger, and 3. we use a different set of absorption features specifically adapted to the LRG sample analysed rather than the full galaxy population analysed by G05. In consequence, our results are complementary to theirs, and provide independent checks on their findings, while at the same time allowing us to extend the results using the larger sample. G05 also found

some discrepant absorption indices poorly matched by the best-fitting models. Our alternative set of models sheds light on the origin of these discrepancies.

Another goal is to quantify the metallicities of the systems and their deviations from solar abundances. Previous studies have suggested that giant ellipticals and LRGs contain super-solar metallicities (Faber 1973; Pickles 1985; Gallazzi et al. 2005), with indications of  $\alpha$ -enhanced abundances (Worthey et al. 1992; Davies et al. 1993; Trager et al. 2000b,a; Eisenstein & et al. 2003), although agreement is not universal (Kelson et al. 2006). The galaxies also show a trend of increasing metallicity with velocity dispersion or mass (Trager et al. 2000a; Caldwell et al. 2003; Thomas et al. 2005; Kelson et al. 2006). Little attention has been devoted to the modelling of the metallicity distribution of early type galaxies. In Section 4, we present models incorporating into standard closed box and accreting box models the sudden quenching of star-formation, as may occur if Active Galactic Nuclei heat the gas, effectively shutting down gas cooling, to describe the evolution of metallicity. We find that the measured metallicity distribution provides added support to the star-formation quenching scenario in the context of these enrichment models.

In the next section, we discuss the sample selected. In Section 3, we describe our methods. Results from the analysis are presented in Section 4. A discussion of the results and conclusions are provided in Section 5.

## 2 SAMPLE SELECTION

The spectra used in this analysis are taken from the Sloan Digital Sky Survey Data Release 4 (DR4) (Adelman-McCarthy & et al. 2006). The SDSS is a five-band imaging survey of the northern Galactic gap, combined with an extensive spectroscopic follow-up program. The spectra cover a large wavelength range (3800–9200 Å) at high resolution  $\lambda/\Delta\lambda \sim 1800$  taken with 3 arcsec diameter fibres. The target spectra are selected using the Luminous Red Galaxy (LRG) cuts as defined in Eisenstein & et al. (2001). The aim of the SDSS LRG survey was to produce a ‘volume-limited’ sample of intrinsically luminous ( $L \geq 3L^*$ ), intrinsically red galaxies out to redshifts of  $z = 0.5$ . Such a sample is useful as a probe of large scale structure in the Universe. Here we use the data to study the properties of giant elliptical galaxies.

The LRGs are selected from the SDSS database by requiring the `TARGET_GALAXY_RED` flag to be set. An additional cut requires the redshift to fall within the range  $0.15 < z < 0.4$ , with the lower limit in place to ensure that underluminous galaxies do not enter the sample. A velocity dispersion cut is also made, requiring  $70 \text{ km s}^{-1} < \sigma < 450 \text{ km s}^{-1}$ . This initial selection yields a dataset of 24,615 galaxies.

Before detailed analysis was undertaken, each spectrum was blueshifted to its respective rest-frame and resampled in steps of 2 Å to match the resolution of the model spectra. Unlike in DR1, the DR4 spectra are not pre-corrected for foreground Galactic dust extinction. We applied this correction using the maps of Schlegel et al. (1998), combined with an extinction law of Cardelli et al. (1989) and  $R_V = 3.1$ .

All magnitudes used are also first corrected for foreground extinction, using values given in the SDSS database.

Our analysis is based predominantly on fits to five specific absorption indices, defined below in Section 3.2. LRG spectra from the SDSS, however, contain not only absorption features but also emission lines produced by hot, interstellar gas. These lines can contaminate the stellar absorption lines and hence suppress the measured absorption index values. Unlike G05, who estimate the effect of emission lines by fitting a linear combination of template spectra, we choose to simply exclude those galaxies where emission lines are detected within the index passbands. This is done by masking pixels from the index calculation for which the `SP_MASK_EMLINE` flag is set. We also reject pixels which have no data present, no sky information, or bright sky levels (flags `SP_MASK_NODATA`, `SP_MASK_NOSKY` and `SP_MASK_BRIGHTSKY`). After this, an index will only have a measured value if there is more than one unmasked pixel in each of the three defining passbands. To make the final cut, spectra must then have measured values for all five of the matching indices described in Section 3.2. These cuts reduce our sample to 4391 spectra in total. Selecting this subset of galaxies does not systematically affect our results; when parameter estimates are made using a subset of the five fitting indices, the overall distribution of that parameter is the same as when all five indices are present. This suggests our findings for the LRG population as a whole are not much affected by contamination from galaxies with appreciable emission lines. This is expected from the low (few per cent) contribution of actively star-forming galaxies to the LRG population (Roseboom & et al. 2006).

## 3 METHOD

### 3.1 PÉGASE synthetic spectra

To analyse the physical properties of the LRG sample, we use the PÉGASE evolutionary synthesis code (Fioc & Rocca-Volmerange 1997), version 2.0, coupled with a new library of high resolution Kurucz stellar spectra generated by Murphy & Meiksin (2004). With this version of the code, developed by Murphy (2003), we can produce spectra of stellar populations with a resolution of 2 Å in the wavelength range 3000–10000 Å, ideal for comparing with the SDSS spectra. The exceptions are for a subset of cool stars, for which only 20 Å resolution synthetic spectra are available, and similarly for very hot stars, although these tend to be nearly featureless so that high resolution is not crucial. Details of the synthetic spectra used are provided by Murphy & Meiksin (2004) and Murphy (2003).

The PÉGASE code uses the standard PADOVA stellar evolutionary tracks of Bressan et al. (1993), supplemented by those of Althaus & Benvenuto (1997) for low mass stars becoming helium white dwarfs. Pseudo-tracks of thermally pulsing asymptotic giant branch (AGB) stars are constructed following Groenewegen & de Jong (1993). Finally, post-AGB and CO white dwarf tracks are taken from Bloeker (1995) and Schoenberner (1983). The positions in the HR diagram of unevolved low-mass stars are taken from Chabrier & Baraffe (1997). Bruzual & Charlot (2003) find that the PÉGASE predictions for colours and mass-to-light

ratios agree closely with those of their standard population synthesis model for simple stellar populations (SSPs) older than 1 Gyr when the same IMF is adopted.

We note that the evolutionary tracks are computed with solar abundance ratios, while our galaxies are expected to have ratios that differ from the solar values. This will dictate the choice of stellar diagnostics used to constrain LRG properties, and is discussed further in the next section.

We adopt a Salpeter initial mass function (IMF) for masses  $0.1 - 120 M_{\odot}$ . This choice differs from those of K03 and G05, who adopt the Kroupa (2001) and Chabrier (2003) IMFs, respectively. (Several IMFs are provided by Chabrier; the form adopted by Gallazzi et al. was based on *Hipparcos* measurements of disc stars in the Milky Way.) Both groups perform their modelling using the Bruzual–Charlot (Bruzual & Charlot 2003) population synthesis code. Tests reported in Bruzual & Charlot (2003) on simple stellar populations show that the Salpeter IMF predicts a mass-to-light ratio a factor 1.5–2 greater than these other choices, which flatten at the low mass end compared with the Salpeter IMF. For masses above a solar mass, both IMFs are very similar in shape to the Salpeter IMF. Since the light of the LRGs is dominated by more massive stars near the Main Sequence turn-off, we expect that the inferred properties of ages and metallicities will be largely unaffected by the choice of IMF. This is supported by the similar colours produced by the different IMFs (Bruzual & Charlot 2003). Since there are no direct measurements of the IMF in LRGs, we adopt the Salpeter IMF for the sake of its widespread usage.

We also differ from K03 and G05 in the stellar spectral libraries used. While we rely on synthesised stellar spectra to provide near uniform coverage of the space in surface temperature, surface gravity and metallicity, the Bruzual–Charlot code incorporates the measured spectra of stars from the STELIB stellar spectral library (Le Borgne et al. 2003). The STELIB library has the advantage of having been drawn from actual stellar spectra, but at somewhat lower resolution ( $\sim 3 \text{ \AA}$  FWHM). The coverage in metallicity, surface temperature and surface gravity is also not uniform (Bruzual & Charlot 2003; Murphy 2003). Our results may be viewed as complementary to these earlier efforts, in that they test the robustness of the inferred properties of the galaxies to the assumptions made in the population synthesis modelling. We compare our results with those of K03 and G05 and comment on any differences in Section 5. Here we note that restricting the modelling parameters and galaxy sample to those of K03 and G05 results in good agreement with their findings.

### 3.2 Stellar diagnostics

In this study we use absorption indices as stellar diagnostics to model the strength of absorption features in the LRG spectra. The original set of 21 Lick indices is considered (Burstein et al. 1984; Worthey et al. 1994), augmented with the four higher-order Balmer line indices of Worthey & Ottaviani (1997) and the high-resolution  $H\gamma HR$  index of Jones & Worthey (1995). Each index is measured by calculating the equivalent width over a central bandpass, normalised by a pseudo-continuum which itself is defined by two adjacent bandpasses. Previous studies have shown that some indices are sensitive mainly to age, such as the Balmer

lines, while others are primarily sensitive to the metallicity of the stellar population, such as the Fe and Mg indices (Trager et al. 2000b). Errors on the indices are calculated following the method of Cardiel et al. (1998).

In addition, we consider the 4000  $\text{\AA}$  break index  $D(4000)$ , which gives the ratio of the average flux density in the bands 4050–4250  $\text{\AA}$  and 3750–3950  $\text{\AA}$  (Bruzual & Charlot 2003). Also calculated is the narrow-band version  $D_n(4000)$  of Balogh et al. (1999) (4000–4100  $\text{\AA}$  and 3850–3950  $\text{\AA}$ ), which is believed to be considerably less sensitive to reddening effects. The ratio of the strength of the CaII H and K lines, as integrated from 3921–3946  $\text{\AA}$  and 3956–3981  $\text{\AA}$ , is also considered briefly (Stoughton & et al. 2002). Unlike the original Lick index studies, which use analytical fitting functions (Worthey et al. 1994) to model index trends, we follow the same method as G05, directly comparing indices measured from our high resolution synthetic spectra to those from the SDSS.

The stellar spectra used are all based on solar metal abundance ratios. External galaxies, as well as having a range of metallicities, are expected to have varying abundance ratios of  $\alpha$  elements to Fe-peak elements. It is believed that  $\alpha$  elements, which include N, O, Mg, Ca, Na, Ne, S, Si and Ti, are produced predominantly in Type II supernovae, while Fe-peak elements, which include Cr, Mn, Fe, Co, Ni, Cu and Zn, originate mainly in Type Ia supernovae. If this abundance ratio, denoted  $\alpha/\text{Fe}$ , differs from the solar value, then the models may show discrepancies with the data. A remedy for this problem suggested by Thomas et al. (2003) is to combine Mg and Fe indices in varying proportions to give a composite index that is dependent on metallicity, but insensitive to  $\alpha$  enhancement.

In this study we consider the  $[\text{MgFe}]'$  index defined by Thomas et al. (2003),

$$[\text{MgFe}]' = \sqrt{\text{Mg}_6(0.72\text{Fe}5270 + 0.28\text{Fe}5335)} \quad (1)$$

and the two composite indices of Bruzual & Charlot (2003),

$$[\text{Mg}_1\text{Fe}] = 0.6\text{Mg}_1 + 0.4 \log(\text{Fe}4531 + \text{Fe}5015) \quad (2)$$

$$[\text{Mg}_2\text{Fe}] = 0.6\text{Mg}_2 + 0.4 \log(\text{Fe}4531 + \text{Fe}5015) \quad (3)$$

The latter two indices were designed to provide a good match to Bruzual & Charlot (2003) spectra for a broad range of galaxy types, but initial studies here showed that they do not give as good a fit to the LRG spectra compared with our PÉGASE models. For this reason we propose two additional composite indices, designed to be independent of the abundance ratio, whilst also providing observational values consistent with those measured for the LRGs using the PÉGASE model spectra:

$$[\text{Mg}_1\text{Fe}]' = 0.8\text{Mg}_1 + 0.2 \log(\text{Fe}5709 + \text{Fe}5782) \quad (4)$$

$$[\text{Mg}_2\text{Fe}]' = 0.8\text{Mg}_2 + 0.2 \log(\text{Fe}4383 + \text{Fe}5406) \quad (5)$$

Using data from Thomas et al. (2003), Figure 1 shows that the two indices are, in fact, insensitive to changes in  $\alpha$  enhancement.<sup>1</sup> For both indices, this behaviour is almost independent of age or metallicity. In the case of  $[\text{Mg}_1\text{Fe}]'$ ,  $\alpha/\text{Fe}$  insensitivity holds for models older than  $\sim 1$  Gyr, and

<sup>1</sup> The data used in the plot are available electronically at [www-astro.physics.ox.ac.uk/~dthomas](http://www-astro.physics.ox.ac.uk/~dthomas)

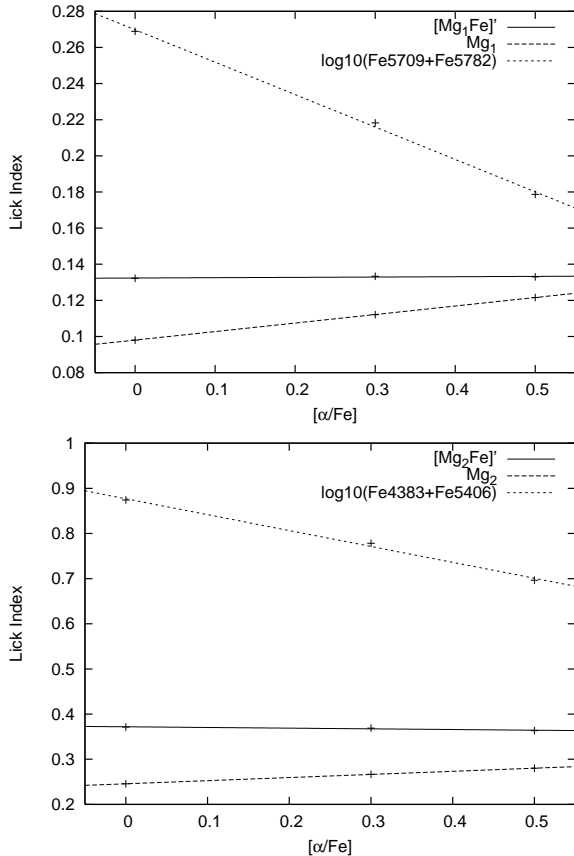


**Figure 1.** Absorption indices as a function of  $\alpha/\text{Fe}$  at fixed overall metallicity. Shown are the new  $[\text{Mg}_1\text{Fe}]'$  (top) and  $[\text{Mg}_2\text{Fe}]'$  (bottom) indices with their constituent Mg and Fe components. Data for the plots comes from Thomas et al. (2003) and is representative of a 12 Gyr old SSP model with solar metallicity (cf. figure 7 of Thomas et al. (2003)).

provides a good metallicity indicator. The  $[\text{Mg}_2\text{Fe}]'$  index is less well behaved, with  $\alpha$  enhancement becoming apparent for models younger than  $\sim 4$  Gyr, especially for low metallicity populations.

To successfully extract age and metallicity information from the SDSS spectra, we choose to simultaneously fit age-sensitive and metal-sensitive indices that are both well reproduced by our models and that show a weak  $\alpha/\text{Fe}$  dependence. After extensive studies fitting a variety of index combinations from PÉGASe to those from the LRG sample, we settle on the following set of indices to be used in the final analysis. The indices  $[\text{MgFe}]'$  and  $[\text{Mg}_1\text{Fe}]'$  are chosen for their sensitivity to metallicity. It was decided that  $[\text{Mg}_2\text{Fe}]'$  should not be used as it is too dependent on  $\alpha/\text{Fe}$  and does not provide an adequate fit to our models. For age sensitive indices we choose  $\text{H}\beta$ ,  $\text{H}\gamma_F$  and  $\text{D}_n(4000)$ . Despite the fact that  $\text{H}\gamma_F$  has been shown to be sensitive to element abundance ratios (Thomas et al. 2003; Korn et al. 2005), including it does not systematically affect our results.

### 3.3 Star formation library

We adopt a Bayesian statistical approach to derive the star formation histories, metallicities and masses for each galaxy

in our sample. The method is similar to the one described in K03 and G05, where the data are assumed to be drawn from a distribution of models, each described by a parameter vector  $\vec{P}$ . A likelihood distribution of a given parameter may be obtained by comparing the observational data with a set of models that populate the space of all possible  $\vec{P}$ . This set of models follows a prior distribution that represents any knowledge of various  $\vec{P}$  values in the absence of any data.

As in K03, we generate a library of 31000 Monte Carlo realizations of different star formation histories. Our models are characterised by an underlying model where stars have been forming according to the exponential law  $\text{SFR} \propto \exp(-\gamma t)$  since time  $t_{\text{form}}$ . Random bursts are then superimposed on this continuous model, and can occur at any time after  $t_{\text{form}}$  with equal probability.

Some of our parameter choices differ from those of K03 and G05 both because our analysis is restricted to LRGs rather than the broad range of galaxy types considered in these earlier studies, and to allow a wider possible range in the prior. We take  $t_{\text{form}}$  to be uniformly distributed between 13.5 and 1.5 Gyr and  $\gamma$  over the interval 0 to 2. This differs from G05, who take  $\gamma$  between 0 and 1. We also set the fraction of models that have experienced a burst in the last 2 Gyr to 1 per cent, compared with 20 per cent used by K03 and 10 per cent used by G05. The implications of changing these priors is discussed in Section 4.4. During a burst, stars can form at a constant rate for a time  $t_{\text{burst}}$ , uniformly distributed from  $3 \times 10^7$  to  $3 \times 10^8$  yr. The mass of stars formed in a burst,  $M_{\text{burst}}$ , is characterised by  $A = M_{\text{burst}}/M_{\text{cont}}$ , where  $M_{\text{cont}}$  is the total mass of stars formed by the continuous model.  $A$  is distributed logarithmically in the range 0.03 to 4.0. The metallicity of the models is logarithmically distributed from  $0.02 - 2.5Z_{\odot}$  and is permitted to take on different values for the continuous model and burst. In most cases, however, for simplicity we shall quote the overall light-weighted metallicity of the model.

Multiple versions of each model are then constructed by gaussian smoothing the spectra to mimic the stellar velocity dispersion of a galaxy. In the range  $150 < \sigma < 300 \text{ km s}^{-1}$ , spectra are smoothed at  $10 \text{ km s}^{-1}$  intervals, rising to  $20 \text{ km s}^{-1}$  for  $300 < \sigma < 450 \text{ km s}^{-1}$ . These intervals are chosen so that over 95 per cent of LRG spectra have a velocity dispersion measurement that lies within one standard deviation of a model value. (The mean velocity dispersion error for the sample is always larger than  $20 \text{ km s}^{-1}$ .) This gives us a total of 23 libraries, each smoothed with a different velocity dispersion and each containing 31000 star formation histories.

For each spectrum in these libraries, we compute the strengths of the  $\text{H}\beta$ ,  $\text{H}\gamma_F$ ,  $\text{D}_n(4000)$ ,  $[\text{MgFe}]'$  and  $[\text{Mg}_1\text{Fe}]'$  indices. The apparent  $u$ ,  $g$ ,  $r$ ,  $i$  and  $z$  magnitudes are calculated using SDSS filters at redshifts between 0.15 and 0.4 in intervals of 0.01. Unless otherwise stated, we assume a flat Friedmann-Robertson-Walker cosmology, with  $\Omega_m = 0.25$ ,  $\Omega_{\Lambda} = 0.75$  and  $H_0 = 73 \text{ km s}^{-1} \text{ Mpc}^{-1}$ .

### 3.4 Parameter estimation

The probability density functions (PDFs) of various physical parameters are calculated by comparing our set of index strengths for a single galaxy to every model spectrum in the library. First of all we select the library with the velocity

dispersion closest to the observed value. Each model is assigned a weight  $w = \exp(-\chi^2/2)$ , where  $\chi^2$  is calculated as follows:

$$\chi^2 = \sum_{i=1}^{i=5} \left( \frac{I_i^{\text{mod}} - I_i^{\text{obs}}}{\sigma_I} \right)^2, \quad (6)$$

where  $I_i^{\text{mod}}$ ,  $I_i^{\text{obs}}$  and  $\sigma_I$  are the model index, observed index and error values respectively. The sum runs over all five indices in our set. The PDF of a particular parameter is then given by the distributions of the weights  $w$  of all the models in the library. We characterize these distributions using the mode (the peak of the distribution) and the median. Errors are often quoted using the 16 – 84 percentile range of the PDF, corresponding to  $\pm 1\sigma$  for a gaussian distribution.

In Figure 2, we show some examples of spectra from the LRG sample, with the model spectrum that gives the best fit based on our set of five indices. In general the best fitting spectrum reproduces many of the absorption features correctly. However, as we only fit absorption indices, the overall shape of the continuum is less well reproduced, especially towards the red end of the spectrum. The strength of this method is that we can derive the star formation history independently of the shape of the continuum and the extinction model. We only need an estimate of the dust extinction when computing mass estimates.

To characterize the age of each galaxy in our library, we calculate the bolometric light-weighted age

$$t_L = \frac{\int_0^t SFR(t-\tau)L(\tau)\tau d\tau}{\int_0^t SFR(t-\tau)L(\tau)d\tau}, \quad (7)$$

where  $L(\tau)$  is the bolometric luminosity of the system evolved over a time  $\tau$ . Similarly, we can define a light-weighted metallicity

$$Z_L = \frac{\int_0^t SFR(t-\tau)L(\tau)Z(t-\tau)d\tau}{\int_0^t SFR(t-\tau)L(\tau)d\tau}, \quad (8)$$

where  $Z(t-\tau)$  is the metallicity of the stars at the time  $t-\tau$ . The metallicity may also be written as  $[Z/H] = \log(Z/Z_\odot)$ , where  $Z_\odot = 0.02$ . In this study we will refer to these quantities as the age and metallicity of a model, respectively.

To estimate the stellar mass of a galaxy, we first need to calculate the effect of dust on the spectrum. Here we model the dust as a simple slab of material between us and the galaxy. Any light,  $S(\lambda)$ , from the galaxy is attenuated according to the following wavelength-dependent law,

$$S_{\text{obs}}(\lambda) = S_{\text{emit}}(\lambda) \times 10^{-0.4 \times A_\lambda} \quad (9)$$

where  $A_\lambda$  is given by the extinction curve of Cardelli et al. (1989). This empirical model takes the following two-component form:

$$\frac{A_\lambda}{A_V} = a(\lambda) + \frac{b(\lambda)}{R_V} \quad (10)$$

where  $a(\lambda)$  and  $b(\lambda)$  are pre-determined polynomials. We adopt the standard Milky Way value of  $R_V = 3.1$  when fitting dust models to the data. This gives essentially a single-component dust model, characterised by  $A_V$ , the attenuation in the V-band (centred on 5500 Å). We infer the value of  $A_V$  using the difference between the fibre  $r-i$  colour and the  $r-i$  colour of each model at a redshift matching the data,

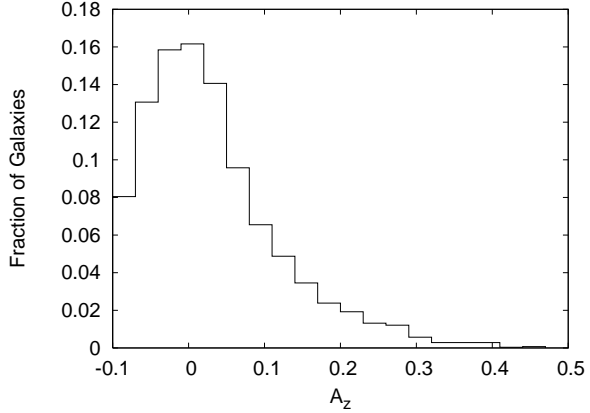


**Figure 3.** The distribution of dust attenuation values in the  $z$  band for the 4391 LRGs in our sample.

$$A_V = \frac{(r-i)_{\text{fibre}} - (r-i)_{\text{model}}}{\left[ a(r) + \frac{b(r)}{R_V} \right] - \left[ a(i) + \frac{b(i)}{R_V} \right]}. \quad (11)$$

Using equation 10, we then calculate the extinction-corrected, photometric  $z$ -band luminosity of the entire galaxy. The stellar mass for a given model can be estimated as follows,

$$M_* = L_z \times \left( \frac{M_*}{L_z} \right)_{\text{model}}, \quad (12)$$

where  $(M_*/L_z)_{\text{model}}$  is the redshifted mass-to-light ratio in the  $z$ -band. This assumes that the mass-to-light ratio within the fibre is the same as for the overall galaxy. G05 find no significant trend of age or metallicity with the fraction of total light entering the fibre for massive early-type galaxies, so this seems a fairly safe assumption. The mass values for each model are then weighted as usual to give a PDF for the stellar mass. As in G05, we allow attenuations down to  $A_z = -0.1$  to account for errors in measurements and discrepancies within the models. Figure 3 shows the distribution of median  $A_z$  values for our sample of SDSS LRGs. The typical attenuation in the  $z$  band is quite small, with a median value of  $2.6 \times 10^{-3}$ . This is consistent with the picture of LRGs as early-type galaxies containing old stellar populations with little dust and gas.

## 4 RESULTS

We now apply the above analysis to the SDSS sample of 4391 Luminous Red Galaxies as described in Section 2.

### 4.1 Index fitting

Figure 4 shows the distribution of indices in the LRG sample when fitted with the final set of indices, using the method described in Section 3.3 (cf., figure 18 of Bruzual & Charlot (2003)). While this plot shows that many indices agree very well with models (e.g.  $[\text{MgFe}]'$ ,  $[\text{Mg}_1\text{Fe}]'$ , Ca4227, Fe5782,  $\text{H}\beta$ ,  $\text{H}\gamma_F$ ,  $\text{D}_n(4000)$ ) others show complete failure (e.g. C24668, NaD,  $\text{H}\delta_A$ ). Thomas et al. (2003) and Korn et al. (2005) investigate the effect of varying individual element abundances on the Lick indices. Thomas et al. (2003) find

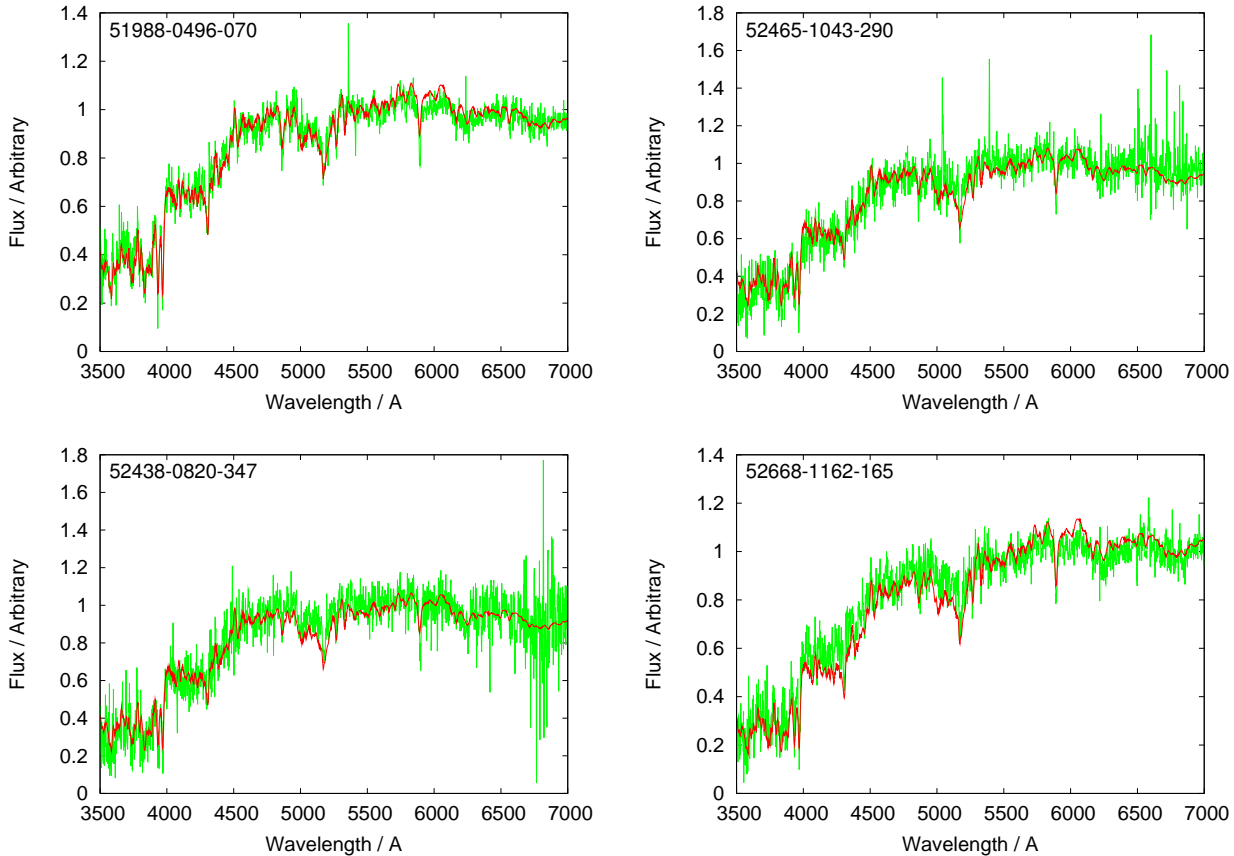


**Figure 2.** Examples of LRG spectra from the SDSS are shown in green, after dereddening for Milky Way extinction. The PÉGASE spectra from the Monte Carlo library with the best-fitting set of the selected five absorption indices (see text) are overplotted in red. Top-Left: The best fit shows a young population with a light-weighted age of 3.5 Gyr and metallicity  $Z = 0.03$ . Top-Right: An example of an old population that formed 9.9 Gyr ago, which experienced a significant burst 1.7 Gyr ago. The best-fit metallicity is  $Z = 0.02$ . Bottom-Left: An example of a spectrum that our method finds a good fit for despite a low SNR (6.3). The galaxy is 5.7 Gyr old with a metallicity of  $Z = 0.03$ . Bottom-Right: An example of a spectrum for which our library fails to find a good fit. The best fitting set of indices gives  $\chi^2 = 19.7$  for five degrees of freedom. The previous three spectra have  $\chi^2 = 4.7, 5.2, 2.0$  respectively. The model spectra have been smoothed slightly for presentation.

that model predictions for  $C_{24668}$  poorly reproduce globular cluster data, even when  $Mg_1$ ,  $CN_1$  and  $CN_2$  are well-modelled. Korn et al. (2005) find this index is most sensitive to the carbon abundance. They also find that the  $NaD$  index is sensitive to both sodium and metallicity and  $H\delta_A$  is affected by iron abundance and metallicity. The narrower passband of  $H\delta_F$  reduces the sensitivity to iron. The blue indices  $CN_1$ ,  $CN_2$ ,  $Ca4227$ ,  $G4300$ ,  $Ca4455$ ,  $Fe4531$  and  $C_{24668}$ , along with  $TiO_2$ , are known to suffer the worst modelling uncertainties (Korn et al. 2005). Many of the remaining discrepancies are likely caused by overabundances of individual elements that are not accounted for by the PÉGASE model. For instance, the iron index  $Fe5015$  is sensitive to Ti and Mg in addition to iron, and to  $\alpha$  enhancement as well (Thomas et al. 2003). Thomas et al. (2003) also find that the  $Mg_b$  index is sensitive to  $\alpha$  enhancement, more so than are either the  $Mg_1$  or  $Mg_2$  indices, for which the agreement is better, though the spread is still large. The under-prediction of some indices, like  $CN_1$  and  $CN_2$ , is expected for  $\alpha$ -enhanced abundances (Thomas et al. 2003). We discuss the indices further in Section 5.

## 4.2 LRG properties

Here we present the results obtained for the light-weighted age, metallicity and stellar mass of the 4391 Luminous Red Galaxies in our sample. Figure 5 shows the distributions of the median-likelihood estimates of these parameters (left-hand side) and their errors (right-hand side) in the top, middle and bottom panels respectively. The age distribution shows a peak at around 6 Gyr, suggesting the LRGs are comprised of mainly old stellar populations. Typical uncertainties on the age are  $\sigma_t \sim 2$  Gyr, with no galaxies showing errors larger than 3 Gyr. The distributions also indicate an average super-solar metallicity of  $[Z/H] \sim 0.2$ , with a long tail down to  $[Z/H] \sim -0.6$ . Errors in the metallicity measured in individual galaxies are around  $\sigma_{[Z/H]} \sim 0.15$ , extending up to 0.3 for some galaxies. Similar distributions are found for the age and metallicity of early type galaxies by Trager et al. (2000b). Finally, the mass shows a narrow distribution that peaks at  $\log(M_*/M_\odot) \sim 11.5$ . It is fairly well constrained, with a maximum error of  $\sigma_{\log(M_*/M_\odot)} \sim 0.1$ . The high mass of the sample is expected from the LRG high

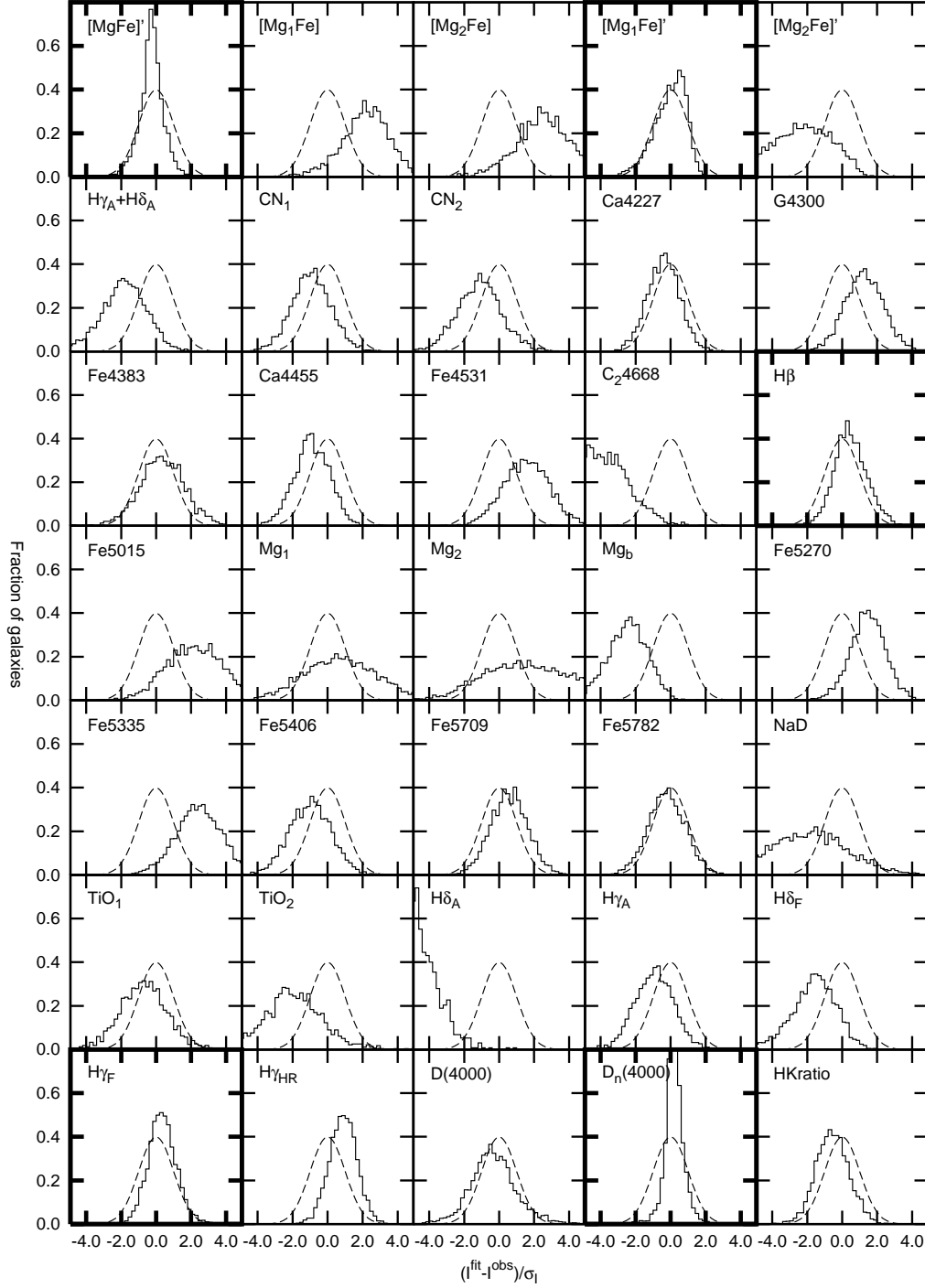


**Figure 4.** Simultaneous fits of the  $\text{H}\beta$ ,  $\text{H}\gamma_{\text{F}}$ ,  $\text{D}_n(4000)$ ,  $[\text{MgFe}]'$  and  $[\text{Mg}_1\text{Fe}]'$  indices (highlighted) of the 4391 galaxies from the SDSS LRG sample with measurable indices. Each panel shows the distribution of the best fitting index  $I^{\text{fit}}$  minus the observed one,  $I^{\text{obs}}$ , divided by the index error  $\sigma_I$ . The dashed line in each panel indicates a gaussian with unit standard deviation.



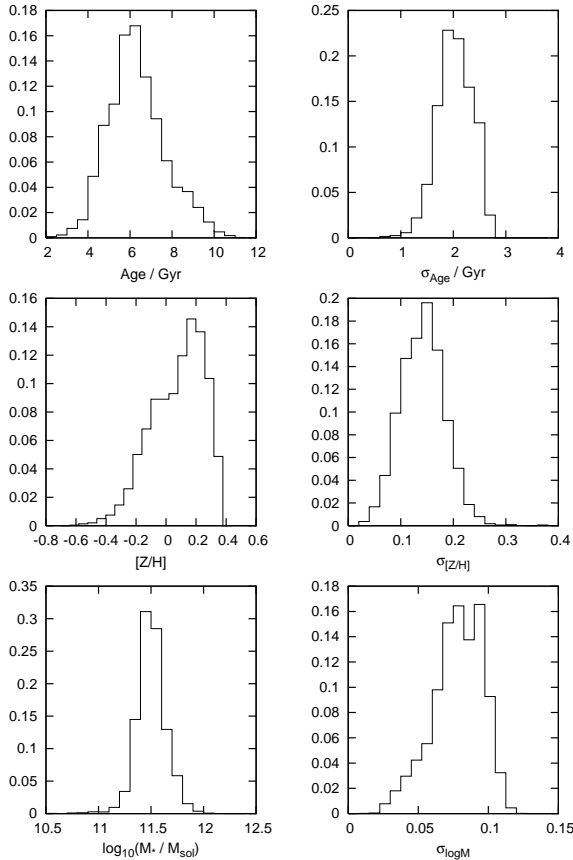


**Figure 5.** Histograms of the median values of age (top-left), metallicity (middle-left) and stellar mass (bottom-left) for 4391 Luminous Red Galaxies from the SDSS-DR4. The y-axis units give the fraction of galaxies in a particular bin. The right-hand panels show the respective error distributions, calculated as one-half of the 16–84 percentile range.

luminosity cuts. The narrow distribution suggests that we have indeed selected a homogeneous population of galaxies.

### 4.3 Age, mass and metallicity relationships

We are also interested in exploring relationships between the mass, age and metallicity of the galaxies in our sample. Rather than simply plot the median of two separate distributions, we calculate the joint distribution of each pair of parameters. This is done by adding the 2D normalised probability distribution of all galaxies in our sample, giving each galaxy equal weight.

In this study, we use the same cosmology as that of De Lucia et al. (2006), who use merger trees from the Millennium Simulation, grafted onto semi-analytic models of galaxy formation, to track the properties of elliptical galaxies. As LRGs are early-type galaxies, we can directly test the predictions of these simulations at the high-mass end using the LRG sample.

In the top-left panel of Figure 6, we show the 2D probability distribution of age against mass. In this plot, the age has been estimated for each galaxy at a redshift of  $z = 0$ , by adding the lookback time to the light-weighted age. Also shown is the distribution of metallicity against stellar mass

in the middle-left. These two plots are comparable to figure 6 of De Lucia et al. (2006), whose predictions for the same variables are shown as the solid and dashed lines, representing the median and upper and lower quartiles respectively.

The plots do not show any strong trends with stellar mass, and reflect the distributions seen in Figure 5. The age appears to be slightly correlated with mass, and suggests that the less massive galaxies are made up of younger stellar populations within the restricted mass range of the LRGs. The metallicity appears to be fairly uniform over the stellar mass range studied, with at most a slight anti-correlation with mass. The slight bimodality in the distribution is discussed further in Section 4.5. The ages predicted by De Lucia et al. (2006) exceed our estimates by 1–3 Gyr. Their metallicity predictions agree closely with ours, although their predicted values are lower by about 0.1 dex.

An issue that invariably arises when deriving galaxy properties is the age-metallicity degeneracy, which occurs due to competition between age and metallicity on absorption-line strengths, so that old, metal-poor galaxies can be mistaken for young, metal-rich ones (or vice versa). Figure 6, bottom-left panel, gives the 2D likelihood distribution of metallicity against light-weighted age (adjusted to  $z = 0$ ), with the degeneracy manifesting itself as an apparent anti-correlation between the two parameters. The bulk of the distribution is centred on ages of 6–7 Gyr and  $[Z/H] \sim 0.2$ , reflecting the 1D distributions in Figure 5. To quantify this degeneracy we calculate the median metallicity in each of the age bins of Figure 6 and fit a straight line through the resulting points. This gives a slope of  $\Delta \log Z / \Delta \log t = -1.05 \text{ dex yr}^{-1}$ .

Previous studies (Caldwell et al. 2003; Kelson et al. 2006) have suggested possible correlations between the age and metallicity of early-type galaxies with velocity dispersion,  $\sigma$ . Kelson et al. (2006) go so far as to claim that the properties of early-type galaxies in clusters can be completely characterised as a one-parameter family, given by the velocity dispersion of the galaxy. The Faber-Jackson relation also motivates investigation into the dependence of mass on velocity dispersion. The right-hand column of Figure 6 shows how the three parameters, age, metallicity and mass, depend on velocity dispersion in our sample. The age seems to show a small correlation with velocity dispersion: the median yields a slope of  $\Delta \text{age} / \Delta \sigma \sim 4 \text{ Myr/kms}^{-1}$ . The metallicity shows an anti-correlation with  $\Delta [Z/H] / \Delta \sigma \sim -1 \times 10^{-3} \text{ dex/kms}^{-1}$ . The mass shows a slight positive correlation of  $\Delta \log(M/M_\odot) / \Delta \sigma \sim 9 \times 10^{-4} \text{ dex/kms}^{-1}$ . The modes of the distribution, however, are well concentrated, centred at about  $240 \text{ km s}^{-1}$ .

### 4.4 Star formation history of LRGs

In addition to deriving the rest-frame parameters of these galaxies, we would like to constrain their star formation histories by tracking the overall star formation rate as a function of cosmic time. To achieve this, we compute the lookback time for each galaxy and extrapolate the past and future star formation histories for each model, weighted in the usual way. This gives us a PDF for star formation rate, in bins of lookback time, which can be summed over the entire sample to give an overall likelihood distribution. It should be

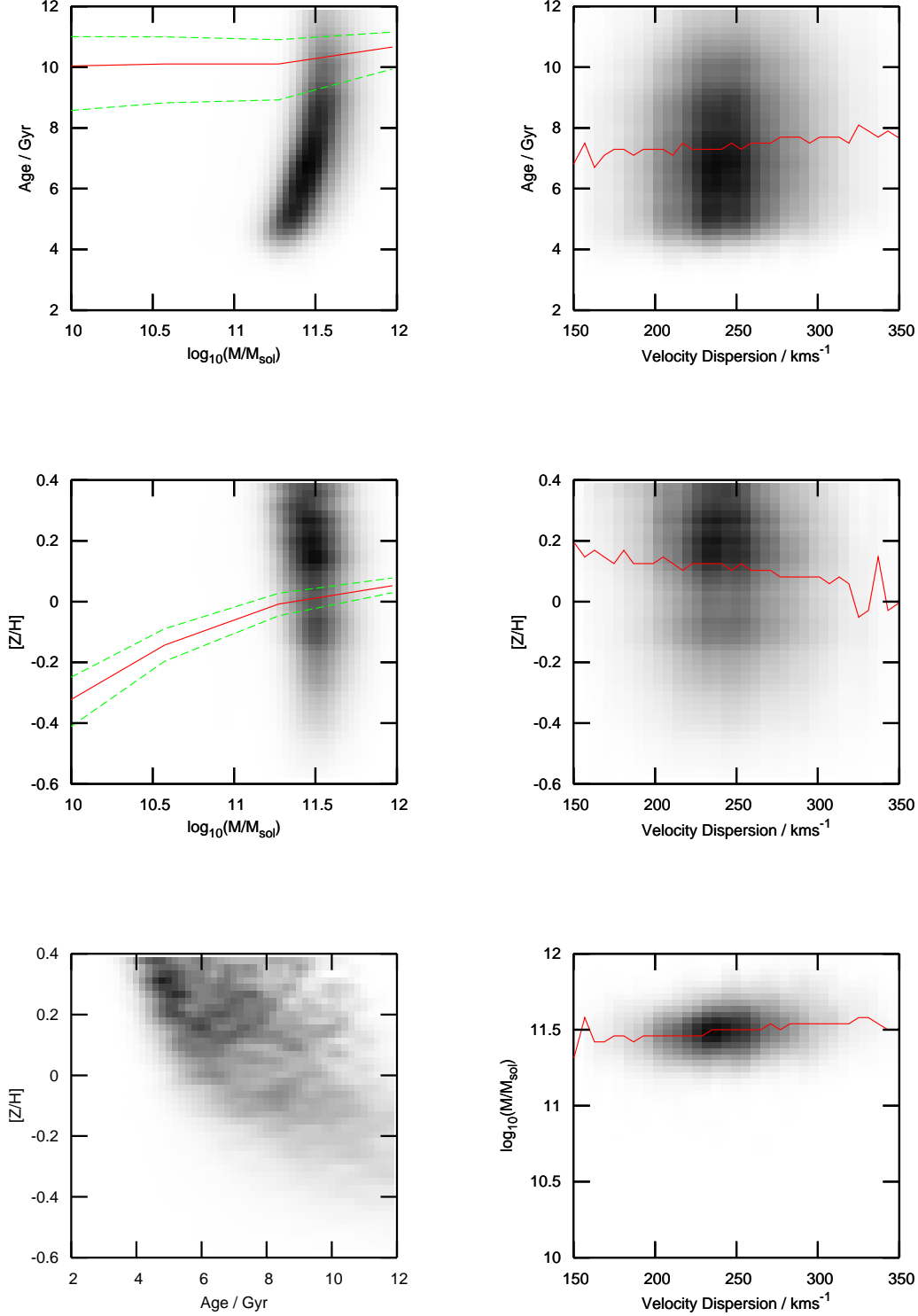


**Figure 6.** Two-dimensional probability distributions for various pairs of galaxy properties. The plots were obtained by adding the normalized 2D distributions for all 4391 galaxies in the SDSS-DR4 sample of LRGs. The left hand-column shows light-weighted age (at  $z = 0$ ) and metallicity against stellar mass, and metallicity against age, from top to bottom respectively. The right-hand column shows age, metallicity and mass against velocity dispersion. The solid line in the upper two plots of the left-hand column shows the median value as predicted by De Lucia et al. (2006), using semi-empirical models. The dashed lines represent the upper and lower quartiles of their distribution. The solid lines in the right-hand column plots give the median parameter value in each velocity dispersion bin.

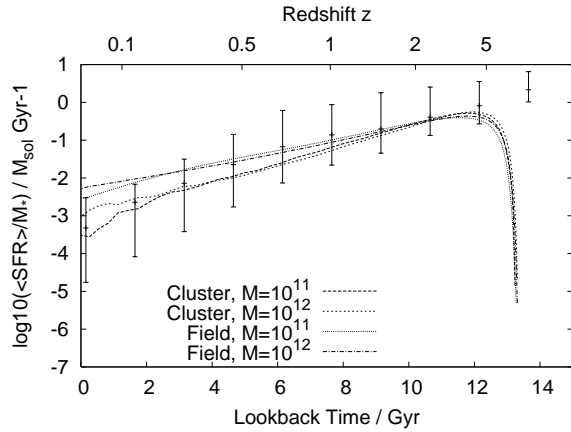


**Figure 7.** The median star formation rate of LRGs in our sample, binned by lookback time. (See text for details.) The continuous lines are the semi-analytic model predictions of De Lucia et al. (2006).

noted that this is only done for the continuous component of the models, and does not include star formation from the burst. We also note that the earlier studies of K03 and G05 used Monte Carlo libraries generated with  $0 < \gamma < 1$  for the continuous component, while here we choose  $0 < \gamma < 2$ . We discuss below the impact of changing this prior on the derived star formation history.

In Figure 7, we present the median values of star formation rate per stellar mass, binned by lookback time. The error bars show the 16th and 84th percentile limits of the distributions in each bin. Also shown is the formation rate from the De Lucia et al. (2006) models (from their figure 1) with stellar masses of  $10^{11} M_{\odot}$  and  $10^{12} M_{\odot}$ , for galaxies in clusters and in the field. For reference, the LRG sample used here is selected in the redshift range  $0.15 < z < 0.4$ , corresponding to lookback times of  $1.8 \text{ Gyr} < t_{lb} < 4.2 \text{ Gyr}$ .

Between lookback times of 3 and 12 Gyr, the LRG results and the simulation show good agreement, with all points lying within the 68-percentile range of the predicted value. For shorter lookback times, the data give a lower star formation rate than expected when compared with simulated field galaxies. In this regime of lookback time, we are extrapolating the future star formation of a galaxy using the passive exponential model and take no account of any possible interactions. This may account for the discrepancy, as additional mergers may boost the star formation rate. Interestingly, there is much better agreement at more recent times when considering galaxies in clusters. This is consistent with the inference that most LRGs reside in clusters (Kormendy & Djorgovski 1989). At lookback times exceeding 12 Gyr, the model curves drop off sharply, while the data still reveal some residual star formation. This is because we only show star formation rates for galaxies with stellar populations existing at these early times. Accordingly, the measured star formation rate at 12 Gyr accounts for only a small fraction of galaxies that will be created in the Universe.

When considering the overall formation mechanism of elliptical galaxies, it is important to distinguish between the *formation times* of the composite stars and the *assembly time* of the constituent progenitors. The formation time of a system can be defined as the time when a certain fraction of stellar mass has been formed, compared with the mass at

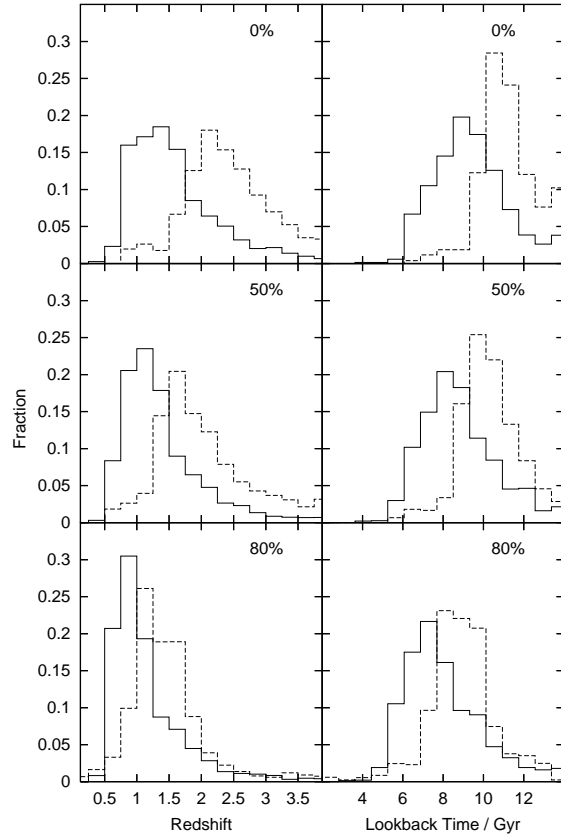


**Figure 8.** The redshift (left-hand column) and lookback time (right-hand column) at the formation time and when 50 per cent and 80 per cent of the stellar mass is in place, compared with the mass at  $z = 0$ . (Top, middle and bottom panels respectively.) The solid line indicates that distribution for a library in which  $0.0 < \gamma < 2.0$ , while the dotted line corresponds to  $0.0 < \gamma < 1.0$ . The lower two distributions (50 per cent and 80 per cent) are comparable to Figure 4 of De Lucia et al. (2006).

$z = 0$ . Here we calculate the cosmic lookback times corresponding to the redshift at which star formation first begins, and when 50 per cent and 80 per cent of the stellar mass has been formed, denoted  $T_{\text{form}}$ ,  $T_{\text{f50}}$  and  $T_{\text{f80}}$  respectively. These parameters give us not only a handle on when the stars in the galaxies formed, but the time-scale over which the stars which reside in LRGs today were forming.

The solid histograms in Figure 8 show the distributions of these formation times and their corresponding redshifts. Table 1 summarizes these results, giving the lower quartile, median and upper quartile values. The results show that the stellar component of LRGs typically first began forming around 8-10 Gyr ago ( $z \approx 1.1 - 1.9$ ), with 80 per cent of the stellar mass in place 6-8 Gyr ago ( $z \approx 0.7 - 1.1$ ).

These values are directly comparable with those provided in table 1 of De Lucia et al. (2006), whose semi-analytic models predict  $T_{\text{f50}} \sim 11 \text{ Gyr}$  and  $T_{\text{f80}} \sim 9 - 10 \text{ Gyr}$ . Our results for  $0 < \gamma < 2$  give ages about 2-3 Gyr younger than the simulation predictions.

In Figure 9 (top), we compare the distribution of the median  $\gamma$ -values when  $0 < \gamma < 2$  is allowed and when the library is restricted to models for which  $0 < \gamma < 1$ . The

|                                                                 |       | 25%   | 50%   | 75%   |
|-----------------------------------------------------------------|-------|-------|-------|-------|
| $0 < \gamma < 2$                                                | Tform | 8.15  | 9.27  | 10.59 |
|                                                                 | Tf50  | 7.52  | 8.58  | 9.97  |
|                                                                 | Tf80  | 6.63  | 7.63  | 9.12  |
| $0 < \gamma < 1$                                                | Tform | 10.38 | 11.08 | 12.14 |
|                                                                 | Tf50  | 9.37  | 10.17 | 11.22 |
|                                                                 | Tf80  | 8.03  | 8.90  | 9.74  |
| De Lucia et al. (2006)<br>( $10.8 < \log(M/M_{\odot}) < 11.5$ ) | Tf50  | 9.78  | 10.56 | 11.22 |
|                                                                 | Tf80  | 7.56  | 9.20  | 10.31 |
| De Lucia et al. (2006)<br>( $11.5 < \log(M/M_{\odot}) < 12.2$ ) | Tf50  | 11.01 | 11.41 | 11.76 |
|                                                                 | Tf80  | 9.50  | 10.31 | 10.79 |

**Table 1.** The lower quartile (25 per cent), median (50 per cent) and upper quartile (75 per cent) values summarizing the lookback times (in Gyr) since formation of LRGs in our sample. Values are shown for the full Monte Carlo library, for which  $0 < \gamma < 2$ , and also the results when the library is restricted to models with  $0 < \gamma < 1$ . For reference, the corresponding values from table 1 of De Lucia et al. (2006) are reproduced here for comparison.

difference in predicted values is striking, with median values of 1.28 and 0.73 for the two distributions, respectively. The impact that this has on the predicted star formation history is shown in Figure 9 (bottom). This plot gives the 2D probability distribution of  $\gamma$  as a function of the time since formation of the galaxy, produced in the same way as Figure 6. We see here that the two parameters appear to be inversely proportional to one another, with older objects having the most prolonged periods of star formation. Generally, only objects older than 7 Gyr are expected to have  $\gamma < 1$ . The overall effect of restricting the prior on  $\gamma$  to  $0 < \gamma < 1$  is therefore to increase the derived ages of the galaxies.

This is illustrated by the dashed histograms of Figure 8 and the corresponding values in Table 1. Here we see that for the more restricted range in  $\gamma$ , the predicted median formation time is increased by 1.8, 1.6 and 1.3 Gyr for Tform, Tf50 and Tf80 respectively. The inter-quartile range for the formation time distributions are reduced from 2.4 Gyr ( $0 < \gamma < 2$ ) to 1.7 Gyr ( $0 < \gamma < 1$ ). This is understandable as by reducing the range of  $\gamma$ , we are also reducing the number of possible star formation histories for a given formation time. Using the more restricted range of  $\gamma$  brings our predictions in closer agreement with those of De Lucia et al. (2006). We note that restricting the prior value of  $\gamma$  also increases the median light-weighted age by 1-2 Gyr, but appears to have little effect on the derived metallicity and mass distributions.

In addition to tracking the formation times of galaxies, it is important to discover whether galaxies have undergone any recent bursts of star formation activity. For each galaxy, we calculate the probability  $p_{\text{burst}}$  of a burst by adding the weights of every model that has experienced a burst in the last  $n$  Gyr, and normalising by the total weight of all models in the library. The distribution of burst probabilities for  $n = 2, 4, 6$  is shown in Figure 10 (bottom panel). The probabilities are generally small. Typically there is only a 0.25 per cent chance of a burst occurring within the last 2 Gyr for an individual galaxy. This rises to 1.6 per cent for bursts within the last 4 Gyr and 3.2 per cent within 6 Gyr. We note that

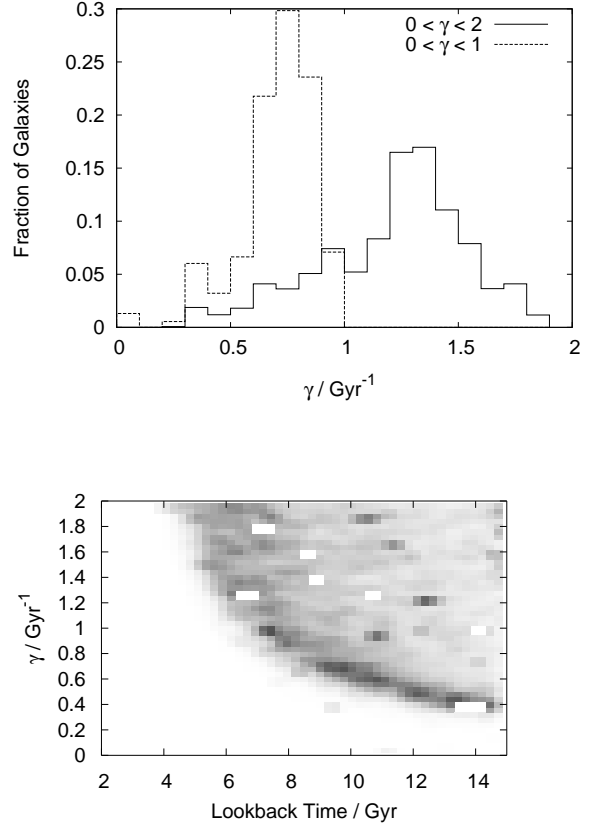


**Figure 9.** The top panel shows the distribution of  $\gamma$  for the LRG sample when the prior range is  $0.0 < \gamma < 2.0$  (solid) and  $0.0 < \gamma < 1.0$  (dashed). The lower panel shows the 2D PDF for  $\gamma$  as a function of the lookback time corresponding to the time of formation.

the burst probabilities may be sensitive to the prior. For reference, we set up the library so that 1 per cent of galaxies experience a burst within the last 2 Gyr. We would also like to calculate the magnitude of these bursts compared with the underlying continuous model. To do this we consider only those models in which bursts have occurred within the lifetime of the galaxy and calculate the median value of  $A = M_{\text{burst}}/M_{\text{cont}}$  by marginalising in the usual way. The top panel of Figure 10 gives a typical value of  $A = 0.4$ , implying that around 29 per cent of the total mass of stars in a galaxy that had a burst in its history would have come from the burst.

#### 4.5 Metallicity of LRGs

In this section, we discuss implications of the measured metallicity distribution of the LRGs in terms of their chemical evolution. The simplest possible model for the chemical evolution of a galaxy is the closed-box model of Talbot & Arnett (1971). We also consider a standard modification allowing for continued accretion of gas by the galaxy. Details of both models are discussed in Binney & Merrifield (1998).

In the closed box model, it is assumed that initially the material is entirely gaseous, possibly enriched to a metallic-

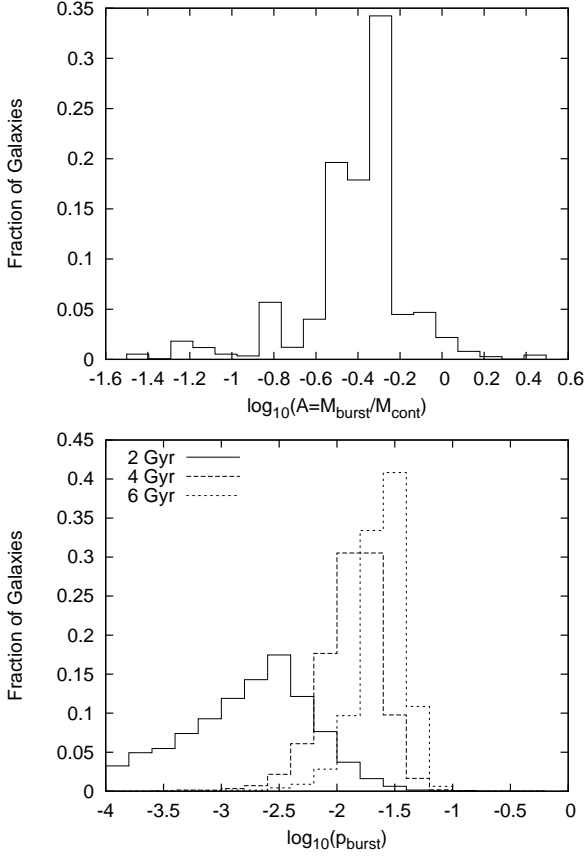


**Figure 10.** The top panel shows the distribution of  $A$ , the ratio of mass formed in a burst compared with that formed by the exponentially decaying model. The lower panel shows the distribution of burst probabilities. The solid, dashed and dotted lines show the distribution of  $p_{\text{burst}}$ , the probability that a galaxy experienced a burst, in the last 2, 4 and 6 Gyr, respectively.

ity level  $Z_i$ . As the name suggests, no material is allowed to enter or leave the region, so there is no further appreciable interaction of the galaxy with its surroundings once it has formed. As the galaxy evolves, stars are formed, consuming interstellar gas in the process and polluting the remaining gas with heavy elements corresponding to a yield  $p$  of mass in metals per mass of stars formed. The yield is assumed constant. It is further assumed that turbulence keeps the gas homogeneous so that the instantaneous recycling approximation may be made, which neglects the delay between the formation of a population of stars and the ejection of heavy elements into the remaining gas by massive stars in the population.

Suppose the interstellar gas has a mass  $\mathcal{M}_g$  and contains a mass of heavy elements  $\mathcal{M}_h$ . The metallicity of the gas is then

$$Z = \frac{\mathcal{M}_h}{\mathcal{M}_g}. \quad (13)$$

In this model, the metallicity may be shown to evolve according to

$$Z(t) = Z_i - p \ln \left[ \frac{\mathcal{M}_g(t)}{\mathcal{M}_g(0)} \right]. \quad (14)$$

The mass of stars in the box with metallicity between  $Z_i$

and  $Z(t)$  is then

$$\begin{aligned} \mathcal{M}_s(< Z) &= \mathcal{M}_s(t) = \mathcal{M}_g(0) - \mathcal{M}_g(t) \\ &= \mathcal{M}_g(0) \left[ 1 - \exp \left( -\frac{Z - Z_i}{p} \right) \right], \end{aligned} \quad (15)$$

and the metallicity distribution of the stars is

$$\frac{d\mathcal{M}_s(< Z)}{dZ} = \frac{\mathcal{M}_g(0)}{p} \exp \left( -\frac{Z - Z_i}{p} \right), \quad (16)$$

for  $Z > Z_i$ , and vanishes for  $Z < Z_i$ . The mean metallicity of the stars is then

$$\begin{aligned} \bar{Z}(t) &= \frac{1}{\mathcal{M}_s} \int_{Z_i}^{Z(t)} Z \frac{d\mathcal{M}_s}{dZ} dZ \\ &= Z_i + p \left( 1 + \frac{x \ln x}{1 - x} \right), \end{aligned} \quad (17)$$

where  $x = 1 - \mathcal{M}_s(t)/\mathcal{M}_g(0) = \exp[-(Z - Z_i)/p]$ . The limiting metallicity values of  $Z = Z_i$  and  $Z \rightarrow \infty$  correspond respectively to  $x = 1$  and  $x = 0$ , and to  $\bar{Z} = Z_i$  and  $\bar{Z} = Z_i + p$ . The mean metallicity is thus restricted to being smaller than the sum of the initial metallicity and the yield. Inspection of Figure 11 suggests the yield must then be as high as  $p \approx 0.05$ .

In this scenario, the distribution of mean metallicity is a reflection of the distribution of initial metallicities  $Z_i$  of the galaxies and their ages, with younger galaxies expected to have lower metallicities on average. However, this picture is not supported by the age-metallicity plot of Figure 6, which, while showing a large amount of scatter for super-solar metallicity values, also shows a general anti-correlation, particularly at low metallicity values. This effect is likely in part due to a residual age-metallicity degeneracy, although the degree to which the degeneracy masks a true underlying trend is unclear.

We next consider a modification of the closed box model in which star formation is abruptly halted after an enrichment phase. The model is motivated by the proposed solution to the anti-hierarchical behaviour of early type galaxies invoking a sudden quenching of star formation in the sub-units which eventually coalesce into the galaxies we see today. In this model, we allow for *stochastic star-formation quenching* (SSQ), modelled as a Poisson process at a uniform rate  $\lambda$ . The probability that star formation is suddenly quenched in any given galaxy between the times  $t$  and  $t + dt$  is then  $\lambda dt$ . The metallicity level any galaxy achieves is then given by the time during which the gas was enriched before star formation ceased, as well as by any initial metallicity. The metallicity distribution is given by

$$\frac{1}{\mathcal{N}_{\text{tot}}} \frac{d\mathcal{N}}{dZ} = e^{-\lambda t} \lambda \frac{dt}{dZ}. \quad (18)$$

The time derivative  $dZ/dt$  requires specifying a star formation rate  $\psi(t)$ . The simplest approximation is a constant rate  $\psi(t) = \psi_0$ . For reasons explained below, we instead consider the more general form

$$\psi(t) = \psi_\beta t^{-\beta}, \quad (19)$$

where  $\psi_\beta$  is a constant and  $0 \leq \beta < 1$ . A constant rate corresponds to the special case  $\beta = 0$ . For  $\beta > 0$ , the rate corresponds to a burst at  $t = 0$ , gradually decaying afterwards. The restriction  $\beta < 1$  ensures a finite mass of stars is formed.

Expressing  $dt/d\bar{Z} = (dt/dx)/(d\bar{Z}/dx)$  and noting  $\psi(t) = d\mathcal{M}_s/dt$  gives

$$x(t) = 1 - \frac{\psi_\beta}{\mathcal{M}_g(0)(1-\beta)} t^{1-\beta}, \quad (20)$$

and

$$\frac{p}{\mathcal{N}_{\text{tot}}} \frac{d\mathcal{N}}{d\bar{Z}} = -\frac{\alpha}{1-\beta} \exp[-\alpha(1-x)^{1/(1-\beta)}] \frac{(1-x)^{\frac{2-\beta}{1-\beta}}}{1-x+\ln x}, \quad (21)$$

where  $\alpha = \lambda[\mathcal{M}_g(0)(1-\beta)/\psi_\beta]^{1/(1-\beta)}$  is the ratio of the gas consumption time-scale to quenching time-scale. Typically this ratio is expected to be large, otherwise most of the mass will have been enriched to its maximum mean value through generations of star formation before star formation ceases.

In the limit of small mean metallicity values,  $\bar{Z} \rightarrow Z_i$ , the distribution function  $(p/\mathcal{N}_{\text{tot}})d\mathcal{N}/d\bar{Z} \rightarrow 2\frac{\alpha}{1-\beta}(1-x)^{\beta/(1-\beta)}$  for  $x \rightarrow 1$ . For the special case  $\beta = 0$ , the limiting value is  $2\alpha$ . This limiting value will in fact apply to any analytic form for  $\psi(t)$  that is non-vanishing at  $t = 0$ , including an exponentially decaying star formation rate. Such asymptotic behaviour, however, is contrary to the diminishing distribution at low metallicity values in Figure 11. For  $0 < \beta < 1$ , the distribution function vanishes for  $\bar{Z} \rightarrow Z_i$ . This is the reason for having introduced this particular ‘cuspy’ form for the decaying burst.

We next modify the simple closed box model by assuming that metal free gas may be accreted by the galaxy from its surroundings. The change in total mass is  $\delta\mathcal{M}_t = \delta\mathcal{M}_s + \delta\mathcal{M}_g \neq 0$ . In this case, the metallicity evolves according to

$$Z(t) = p \left[ 1 - \left( 1 - \frac{Z_i}{p} \right) e^{x-1} \right], \quad (22)$$

where  $x = 1 - M_s(t)/M_g(0)$ , as for the closed box case. The relation between  $x$  and  $t$  is again given by Eq. 20. As there is no upper limit to the amount of gas accreted, there is no upper limit to the amount of stars which may form. As a consequence,  $x$  may become arbitrarily small. In the limit  $x \rightarrow -\infty$ , the metallicity takes on the value of the yield ( $Z \rightarrow p$ ). The maximum metallicity achievable is the yield, provided  $Z_i < p$ . (For  $Z_i > p$ , the metallicity will decrease with time towards  $p$ .)

The mean metallicity evolves according to

$$\bar{Z}(t) = p + \frac{Z(t) - Z_i}{\ln \frac{p-Z(t)}{p-Z_i}}, \quad (23)$$

with the limiting value  $\bar{Z} \rightarrow p$  as  $x \rightarrow -\infty$ . In analogy to the closed box case, the metallicity distribution in the SSQ model is given by

$$\begin{aligned} \frac{p}{\mathcal{N}_{\text{tot}}} \frac{d\mathcal{N}}{d\bar{Z}} &= \frac{\alpha}{1-\beta} \exp[-\alpha(1-x)^{1/(1-\beta)} + 1-x] \\ &\times \frac{(1-x)^{\frac{1}{1-\beta}}}{\frac{Z-Z_i}{1-x} e^{1-x} + Z_i - p}. \end{aligned} \quad (24)$$

Best fits to the measured distribution are shown in Figure 11 (upper panel) for both the closed box (solid line) and accreting box (dashed line) SSQ models. For the closed box SSQ model, the parameters for the fit are  $Z_i = 0.0040$ ,  $\alpha = 66$ ,  $\beta = 0.59$  and  $p = 0.26$ . For the accreting box SSQ model, the parameters for the fit are  $Z_i = 0.0040$ ,

$\alpha = 2.3$ ,  $\beta = 0.50$  and  $p = 0.10$ . Both models well describe the distributions. Error bars are not quoted because neither fit has an acceptable value of  $\chi^2$  (reduced  $\chi^2 \approx 5$ ), due in large part to non-Poisson fluctuations from bin to bin. A dip near solar metallicity hints at a bimodal distribution. Without extensive Monte Carlo tests of the population synthesis model-fitting procedure, it is difficult to assess the statistical significance of the fluctuations, and of any evidence for bimodality. Doing so is beyond the scope of this paper, but may be worth considering in any future estimates of the galaxy metallicity distribution. The spread in parameter values between the two models provides some indication of the errors. We note that the excess number density of systems predicted by the models for  $Z \approx 0.05$  may be an artefact of the stellar library, which is restricted to  $Z \leq 0.05$ .

Values for  $\alpha$  exceeding unity are expected, and confirm the assumption that star formation is quenched on a time-scale short compared with the time-scale for complete conversion of the initial gas mass into stars. Adopting two e-foldings of star formation in the population synthesis models for the conversion time, the distribution of  $\gamma$  in Figure 9 suggests a typical time-scale for depleting the initial gas content of  $2/\gamma \sim 1.5 \times 10^9$  yr. The corresponding quenching time-scale  $\lambda^{-1}$  for the closed box SSQ model is then  $2/\gamma\alpha \approx 2 \times 10^7$  yr, comparable to the Salpeter time ( $t_{\text{Salp}} = \epsilon\sigma_{\text{TC}}/4\pi Gm_p$ ) for a black hole energy conversion efficiency  $\epsilon$  of 5 per cent, and to the lower limit for the lifetime of a luminous QSO (Yu & Tremaine 2002). The effective yield value for the model is quite high, comparable to that expected from massive stars alone (Maeder 1992; Hirschi et al. 2005), and so is not expected for a normal initial mass function. Such an IMF would result almost entirely in stars sufficiently massive to produce Type II supernovae. A metallicity value corresponding to Type II supernovae ejecta is consistent with the evidence for  $\alpha$ -enhanced abundances. An IMF dominated by massive stars should not necessarily be precluded. An initial mass function heavily weighted towards massive stars ( $dN/dm \sim 1/m$ ) has been invoked in recent semi-analytic galaxy formation models to reproduce sub-millimetre galaxy counts and the high metallicities observed in the intracluster gas of rich galaxy clusters (Lacey et al. 2006, in preparation). Luminous Red Galaxies are believed to reside predominantly in the cores of just such rich clusters.

For the accreting box SSQ model, the smaller value for  $\alpha$  corresponds to a star-formation quenching time-scale of  $\sim 6 \times 10^8$  yr, comparable to the upper limit for the lifetime of a luminous QSO (Yu & Tremaine 2002). The effective yield value for the model is still high, about twice that expected for the Chabrier (2003) initial mass function for early stars, for which a little under half of the stellar mass is contained in stars massive enough to form Type II supernovae, and assuming an approximate mean ejected mass fraction of 10 per cent. It suggests again an IMF tilted toward more massive stars, but not as strongly as required by the closed box model.

The sudden star-formation quenching scenario may also account in part for the inverse correlation between age and metallicity. For a given formation time, systems with an extended amount of star formation before quenching will produce stars with increasing metallicity and a younger average population compared with systems in which star formation

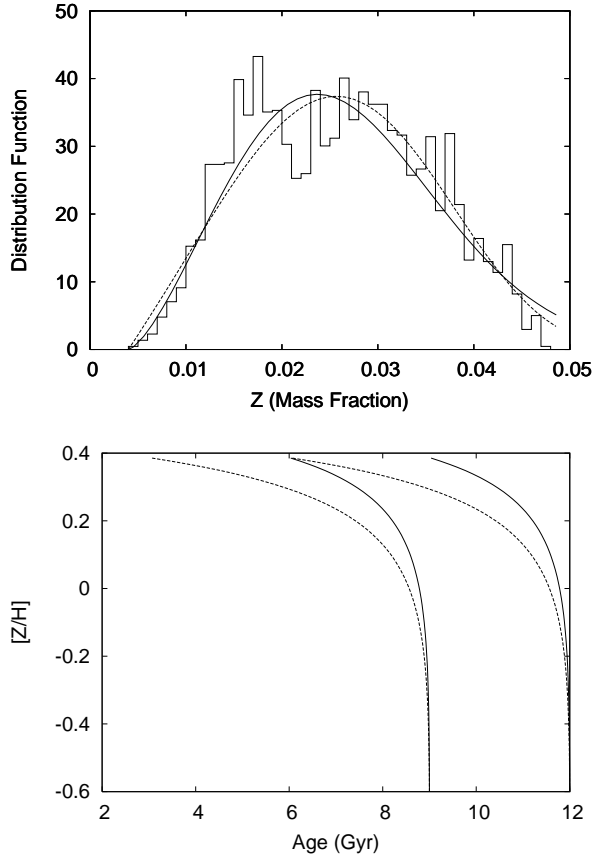


**Figure 11.** The top panel shows the metallicity distribution function for LRGs in our sample (histogram). The solid line is a fit of a closed box SSQ model, while the dashed line is for an accreting box SSQ model (see text). The bottom panel shows the relation between age and metallicity predicted by the accreting box SSQ model for characteristic quenching time-scales of 0.65 Gyr (solid lines) and 1.3 Gyr (dashed lines) for formation times of 9 Gyr and 12 Gyr.

was quenched early. Because of the short characteristic decay time for star formation, however, the ages of the stars will not differ greatly (typically  $\sim 2\gamma^{-1} \approx 1.5$  Gyr), so that the inverse relation must also result from a range in formation times. For slower star formation, however, a broader range in ages is possible. The relation between the lookback time to the time at which star formation was quenched and the mean metallicity of the stars at that time is shown in Figure 11 (lower panel) for the accreting box SSQ model. Values of  $\lambda^{-1} = 0.65$  Gyr (solid lines) and  $\lambda^{-1} = 1.3$  Gyr (dashed lines) are shown, with formation times of 9 Gyr and 12 Gyr. These curves span the range of metallicity vs age in Figure 6. The rapid ascent at low (sub-solar) metallicities, and slower metallicity evolution at higher (super-solar) metallicities, predicted by the model suggests that most galaxies will be concentrated in the region of super-solar metallicities, consistent with the 2D age-metallicity distribution in Figure 6.

## 5 DISCUSSION & CONCLUSIONS

In this section, we compare our results with those in previous works, and summarise the main conclusions of our study. The groups at MPA/JHU have made publically available large catalogues of the results of model fits to SDSS data. These include the mass catalogues of K03 (updated to Data Release 4) and age, mass and metallicity values of G05 (Data Release 2)<sup>2</sup>.

To make our results comparable with values from K03 and G05, the library is restricted to models with  $0 < \gamma < 1$ , to more closely match our prior with theirs. We then recompute masses by fitting only the  $D_n(4000)$  and  $H\delta_A$  indices to allow direct comparison with K03. Similarly, we calculate masses, ages and metallicities by fitting the  $[MgFe]'$ ,  $[Mg_2Fe]$ ,  $H\beta$ ,  $H\gamma_A + H\delta_A$  and  $D_n(4000)$  indices, as used in G05. We also match cosmologies, adopting a flat Friedmann-Robertson-Walker universe with  $\Omega_m = 0.3$  and  $H_0 = 70 \text{ km s}^{-1} \text{ Mpc}^{-1}$ .

The left-hand column of Figure 12 shows a comparison between our values and those from the MPA/JHU catalogue. All derived parameter values show generally good consistency over the ranges studied. The right hand-column of Figure 12 shows the distribution of differences between our values and the MPA/JHU values. The solid histogram uses the modified prior and K03 or G05 indices as above. The dashed histogram shows the same residuals using the full library ( $0 < \gamma < 2$ ) and the original set of indices ( $[MgFe]'$ ,  $[Mg_1Fe]'$ ,  $H\beta$ ,  $H\gamma_F$  and  $D_n(4000)$ ).

The stellar mass distribution we derive is narrowly peaked around  $3 \times 10^{11} M_\odot$ . A comparison between our derived stellar masses and those of K03 shows overall consistency, with a scatter of  $\sim 0.16$  dex. Our stellar mass values are in general larger than theirs by  $\sim 0.09$  dex when using their indices, and  $\sim 0.07$  dex using ours. There is a smaller offset when we compare our masses to those derived by G05:  $\sim 0.02$  dex using their set of indices, and  $\sim -0.04$  dex with ours.

The offsets are likely to be due to a combination of factors. Principal among these is the difference in the adopted initial mass function (IMF). While we use the Salpeter IMF, K03 use the Kroupa (2001) IMF and G05 use that of Chabrier (2003) for disc stars. Bruzual & Charlot (2003) show that, for a simple stellar population with solar metallicity, the Salpeter IMF results in an increased stellar mass-to-light ratio of about 0.2 dex over the Kroupa and Chabrier IMFs, at a given evolutionary time. Our stellar mass values agree with the results of K03 and G05 more closely than this, which on the surface is surprising. The reason for the good agreement appears in fact to be in part fortuitous. The effect of broadening the range of  $\gamma$  to  $0 < \gamma < 2$  is to find ages that are, on average,  $\sim 1.1$  Gyr smaller than those of K03 and G05. If we limit the prior to  $0 < \gamma < 1$ , this difference reduces to  $\sim 0.4$  Gyr. The scatter in ages is around  $\sim 1$  Gyr. According to the results of Bruzual & Charlot (2003), the larger ages found by K03 and G05 correspond to an increase in the mass-to-light ratio of close to 0.1 dex over the values corresponding to our best fits. This difference brings our stellar mass estimates and those of K03 and

<sup>2</sup> Data available electronically at <http://www.mpa-garching.mpg.de/SDSS>

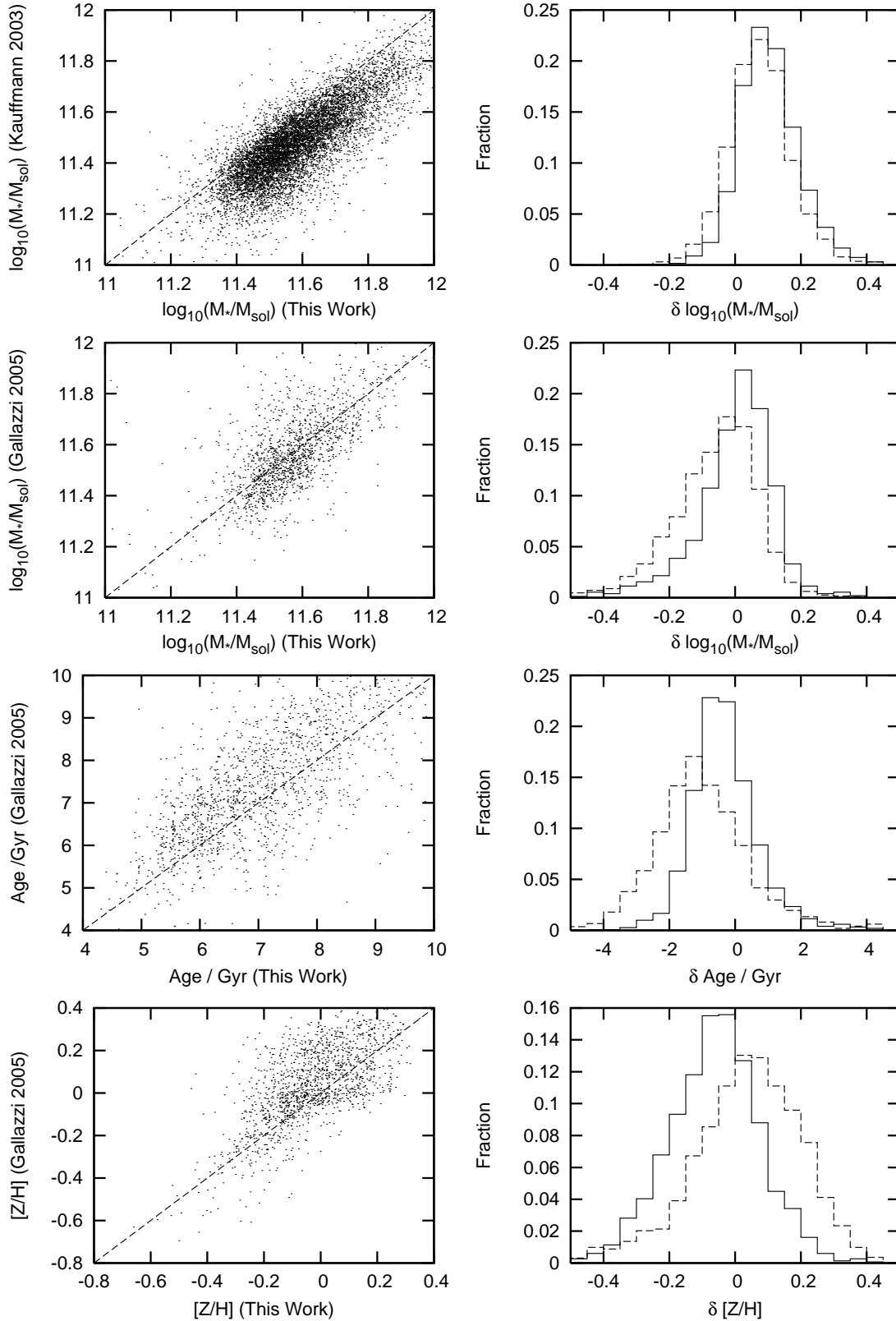


**Figure 12.** Comparison of results from this paper with previous work. The left-hand column shows our stellar mass values against those of K03 and G05 (top two plots), and our age and metallicity against the values of G05 (bottom two plots). The values quoted have been calculated by fitting the similar indices and priors as K03 and G05 respectively. The right hand column shows the residual between our values and the corresponding previous result. The solid histograms use the same indices and similar priors as K03 or G05, while the dashed histograms use our set of indices and Monte-Carlo priors.



G05 into fairly close agreement. Had we adopted the Kroupa (2001) or Chabrier (2003) IMF, the peak in the measured stellar mass distribution would be smaller by about 0.2 dex, or  $2 \times 10^{11} M_{\odot}$ .

When using  $0 < \gamma < 2$ , we also find that our best fitting models are more metal-rich compared with those of G05 by  $\sim 0.05$  dex, with a scatter of  $\sim 0.15$  dex. Our models, however, are comparatively metal-poor by  $\sim 0.05$  dex when using  $0 < \gamma < 1$ . Here we see the age-metallicity degeneracy in effect: younger ages correlate with higher metallicities, and vice versa.

Sources of discrepancy in addition to the difference in priors include the rejection by K03 of models for which the  $r-i$  colour is redder than observed, the difference in the population synthesis techniques adopted to generate the models and the consequent difference in the abilities of the models to reproduce the absorption line features in the spectra. We include models with  $A_z$  attenuations down to  $-0.1$ , following the method of G05. We also note that we are using a different extinction curve to that adopted by K03 and G05, who both use the single power law ( $\propto \lambda^{-0.7}$ ) of Calzetti et al. (1994). The derived  $A_z$  values we find are sufficiently small (see Section 3.4) to have a negligible effect on the mass estimates.

One way to examine the effect of these different choices is to examine how well the two models reproduce the absorption indices. In figure 18 of Bruzual & Charlot (2003), the  $H\beta$ ,  $H\delta_A$ ,  $H\gamma_A$ ,  $D_n(4000)$ ,  $[MgFe]'$ ,  $[Mg_1Fe]$  and  $[Mg_2Fe]$  index strengths are used to fit high signal-to-noise galaxies from the SDSS Early Data Release (EDR). A comparison of this plot with our Figure 4 shows general consistency in the systematic offsets of many indices, despite the broader range in galaxy types modelled by Bruzual & Charlot (2003). For example, both models fit the  $H\beta$ ,  $D_n(4000)$  and  $[MgFe]'$  well, whilst underestimating the strengths of the  $CN_1$ ,  $CN_2$ ,  $Ca4455$ ,  $C24668$ ,  $Mg_b$  and  $NaD$  indices and overestimating  $Fe4383$ ,  $Fe5015$ ,  $Fe5270$  and  $Fe5335$ . This behaviour is encouraging as it allows us to check the consistency of both models. There are some indices that are not consistent, however. For example, we tend to overestimate the strengths of the two magnesium indices,  $Mg_1$  and  $Mg_2$ , while the Bruzual & Charlot (2003) models underestimate them. Other indices that show differences are  $Ca4227$ ,  $G4300$ ,  $Fe4531$ ,  $Fe5406$ ,  $TiO_1$ ,  $TiO_2$  and  $H\delta_A$ . These differences are likely in part due to the differences in the galaxy populations modelled.

The results of Section 4.4 highlight an important consideration when setting up this type of analysis, namely what range should  $\gamma$  take in the prior? We have shown here that doubling the upper limit of  $\gamma$  from 1 to 2 decreases the formation redshift considerably from  $z \sim 2.0$  to  $z \sim 1.0$ , making the derived ages younger by around 2 Gyr. This anti-correlation between  $\gamma$  and time since formation shown in Figure 9 is an example of the degeneracy between formation epoch and formation time-scale. So an old, slowly-forming galaxy would appear similar to a young galaxy that formed over a relatively short time-scale. Thomas et al. (2005) claim that this degeneracy could be lifted by relating observationally derived  $\alpha/Fe$  ratios with their time-scales. Their simulations predict that an early-type galaxy of mass  $M_*/M_{\odot} \sim 10^{11.5}$ , should have formed on a time-scale of roughly 260 Myr. In their study, gaussians are used as a toy

model of star formation histories, whereas we use decaying exponentials. Approximating their formation time-scale as the inverse of  $\gamma$  gives  $\gamma \sim 3.8 \text{ Gyr}^{-1}$ . This suggests that perhaps an even larger range of  $\gamma$  is required to cover the full range of physical star formation histories. It appears, though, that the range we use works well for most of the galaxies. The distribution of  $\gamma$  values in the upper panel of Figure 9 shows a gradual decline towards the upper limit for the  $0 < \gamma < 2$  fits. This is in contrast to a crowding of  $\gamma$  values towards the upper limit for the  $0 < \gamma < 1$  fits. This suggests that, while some galaxies may be better fit by models with  $\gamma > 2$ , the range  $0 < \gamma < 2$  well describes the bulk of the LRG population.

We also check the consistency of our results by comparing the trends shown by the 2D probability distributions of Figure 6 with previous studies. Figure 12 of G05 shows similar distributions of stellar metallicity and age for early-type galaxies in their sample. We are interested in the upper mass bin, where  $\log(M/M_{\odot}) > 11$ . They find that the high mass galaxies occupy a region of parameter space centred on an age of about 8 Gyr and metallicity of  $[Z/H] = 0.1 - 0.2$ . This is roughly consistent with the age-metallicity plot in Figure 6, which covers a similar region. Both plots also show a similar age metallicity-degeneracy trend, with a slope of  $\Delta \log Z / \Delta \log t = -1.05 \text{ dex yr}^{-1}$  from our plot, compared with the value of  $-0.75 \text{ dex yr}^{-1}$  found by G05. There are, however, some differences. We find ages smaller than theirs by about 1–2 Gyr and slightly higher metallicities. Our Figure 12 demonstrates that these differences are due primarily to our different choice of indices to fit and Monte-Carlo priors in the construction of the library of template spectra.

Only a small percentage of the spectra are better fit by including a burst on top of the continuous star formation. The probability that a galaxy experienced a burst within the past 6 Gyr of its life is about 3 per cent, and only about 0.25 per cent within the past 2 Gyr. This may in part be due to our selection criterion of avoiding spectra with emission lines, but it is consistent with the small percentage of LRGs showing evidence of recent star formation found by Roseboom & et al. (2006). For those galaxies better fit by the addition of a burst, the burst contributes 20–40 per cent of the total stellar mass of the galaxy.

There have been a number of studies that show a distinct trend between the properties of early-type galaxies and their velocity dispersions. Caldwell et al. (2003) derive the ages and metallicities of 175 nearby, early-type galaxies using a combination of index-index grids. They find a correlation between age and  $\sigma$ , with a  $230 \text{ km s}^{-1}$  (the upper limit on their observations) galaxy expected to have an age between 4 and 14 Gyr and a metallicity range of  $-0.2 < [Z/H] < 0.3$ . Both of these results are broadly consistent with our findings, and suggest that we are studying too narrow a range in velocity dispersion or too homogeneous a population to detect any significant trend.

The evolution in the median star formation rate we infer for the LRGs agrees well with the semi-analytic galaxy formation predictions of De Lucia et al. (2006). We agree less well on the formation times. Comparing the times at which either 50 per cent or 80 per cent of the stars in the LRGs were formed gives times shorter by about 2 Gyr from the predictions of the semi-analytic models. We also find metallicities about 0.15–0.2 dex larger than predicted.

In an attempt to understand the origin of the metallicity distribution of the galaxies, we introduce a stochastic star-formation quenching model for the metallicity evolution. In this model, metallicity evolves either as a closed box or an accreting box, up until a time when star formation abruptly ceases. The model is motivated by quenching scenarios invoked to resolve the ‘anti-hierarchical’ formation problem, such as the shutting-off of gas cooling by AGN activity. We find that while no model provides a perfect fit to the data, the underlying measured distribution is well-described by both the closed box and accreting box versions, provided a ‘cuspy’ burst of star-formation is adopted. The characteristic time-scale for quenching the star formation is around  $10^8$  yr, comparable to the estimated lifetimes of luminous QSOs. The required effective yield values, however, are quite different. For the closed box model, a yield of about 0.26 is required. Such a high yield requires the enrichment to be dominated by very massive stars. Such a possibility, however, should perhaps not be discarded and is being considered in a newer set of semi-analytic models (Lacey 2006, in preparation). For the accreting box, a more moderate yield of about 0.10 is required. This is still about twice the yield expected for the Chabrier (2003) IMF for early stars, and again suggests an IMF more strongly weighted towards higher masses. The dominant role Type II supernovae would play in determining the abundances for such IMFs is consistent with the  $\alpha$ -enhanced abundances inferred from the absorption indices of LRGs.

The quenching model also predicts an anti-correlation between the ages of the stars today and their metallicities, as early quenching will result in older stars with smaller metallicities for a given formation time. This provides a physical basis to the observed anti-correlation, which may thus not solely be an artefact of the age-metallicity degeneracy affecting population synthesis modelling. The relation, however, will also depend on the range of formation times and decay times for the star formation. Such effects are perhaps best accounted for in semi-analytic galaxy formation models. Here we suggest that the distribution of metallicity and the anti-correlation with age should provide further constraints on such models.

## ACKNOWLEDGMENTS

TB would like to thank the Royal Society of Edinburgh for their support through a Robert Cormack Bequest Scholarship. TB would also like to thank the School of Physics at the University of Edinburgh for making this research possible.

## REFERENCES

Adelman-McCarthy J. K., et al. 2006, *ApJS*, 162, 38  
 Althaus L. G., Benvenuto O. G., 1997, *ApJ*, 477, 313  
 Balogh M. L., Morris S. L., Yee H. K. C., Carlberg R. G., Ellingson E., 1999, *ApJ*, 527, 54  
 Baugh C. M., Cole S., Frenk C. S., Lacey C. G., 1998, *ApJ*, 498, 504  
 Binney J., Merrifield M., 1998, *Galactic Astronomy*. Princeton University Press, Princeton, NJ

Bloeker T., 1995, *A&A*, 299, 755  
 Blumenthal G. R., Faber S. M., Primack J. R., Rees M. J., 1984, *Nature*, 311, 517  
 Boselli A., Gavazzi G., Donas J., Scodreggio M., 2001, *AJ*, 121, 753  
 Bower R. G., Benson A. J., Malbon R., Helly J. C., Frenk C. S., Baugh C. M., Cole S., Lacey C. G., 2006, *MNRAS*, 370, 645  
 Bressan A., Fagotto F., Bertelli G., Chiosi C., 1993, *A&AS*, 100, 647  
 Brinchmann J., Charlot S., White S. D. M., Tremonti C., Kauffmann G., Heckman T., Brinkmann J., 2004, *MNRAS*, 351, 1151  
 Bruzual G., Charlot S., 2003, *MNRAS*, 344, 1000  
 Bundy K., Ellis R. S., Conselice C. J., 2005, *ApJ*, 625, 621  
 Bundy K., Ellis R. S., Conselice C. J., Taylor J. E., Cooper M. C., Willmer C. N. A., Weiner B. J., Noeske K. G., Eisendardt P. R. M., , 2005, preprint, astro-ph/0512465  
 Burstein D., Faber S. M., Gaskell C. M., Krumm N., 1984, *ApJ*, 287, 586  
 Caldwell N., Rose J. A., Concannon K. D., 2003, *AJ*, 125, 2891  
 Calzetti D., Kinney A. L., Storchi-Bergmann T., 1994, *ApJ*, 429, 582  
 Cardelli J. A., Clayton G. C., Mathis J. S., 1989, *ApJ*, 345, 245  
 Cardiel N., Gorgas J., Cenarro J., Gonzalez J. J., 1998, *A&AS*, 127, 597  
 Chabrier G., 2003, *PASP*, 115, 763  
 Chabrier G., Baraffe I., 1997, *A&A*, 327, 1039  
 Cimatti A., Daddi E., Renzini A., , 2006, preprint, astro-ph/0605353  
 Cole S., Aragon-Salamanca A., Frenk C. S., Navarro J. F., Zepf S. E., 1994, *MNRAS*, 271, 781  
 Conselice C. J., 2006, *ApJ*, 638, 686  
 Cowie L. L., Songaila A., Hu E. M., Cohen J. G., 1996, *AJ*, 112, 839  
 Davies R. L., Sadler E. M., Peletier R. F., 1993, *MNRAS*, 262, 650  
 Davis M., Efstathiou G., Frenk C. S., White S. D. M., 1985, *ApJ*, 292, 371  
 De Lucia G., Springel V., White S. D. M., Croton D., Kauffmann G., 2006, *MNRAS*, 366, 499  
 Dekel A., Birnboim Y., 2006, *MNRAS*, 368, 2  
 Drory N., Salvato M., Gabasch A., Bender R., Hopp U., Feulner G., Pannella M., 2005, *ApJ*, 619, L131  
 Eisenstein D. J., et al. 2001, *AJ*, 122, 2267  
 Eisenstein D. J., et al. 2003, *ApJ*, 585, 694  
 Faber S. M., 1973, *A&AS*, 10, 201  
 Fioc M., Rocca-Volmerange B., 1997, *A&A*, 326, 950  
 Fontana A., Pozzetti L., Donnarumma I., Renzini A., Cimatti A., Zamorani G., Menci N., Daddi E., Giallongo E., Mignoli M., Perna C., Salimbeni S., Saracco P., Broadhurst T., Cristiani S., D’Odorico S., Gilmozzi R., 2004, *A&A*, 424, 23  
 Gallazzi A., Charlot S., Brinchmann J., White S. D. M., Tremonti C. A., 2005, *MNRAS*, 362, 41  
 Gavazzi G., Boselli A., Pedotti P., Gallazzi A., Carrasco L., 2002, *A&A*, 396, 449  
 Groenewegen M. A. T., de Jong T., 1993, *A&A*, 267, 410  
 Heyl J., Colless M., Ellis R. S., Broadhurst T., 1997, *MNRAS*, 285, 613

- Hirschi R., Meynet G., Maeder A., 2005, *A& A*, 433, 1013
- Jones L. A., Worthey G., 1995, *ApJ*, 446, L31
- Kauffmann G., 1996, *MNRAS*, 281, 487
- Kauffmann G., Charlot S., 1998, *MNRAS*, 294, 705
- Kauffmann G., Heckman T. M., White S. D. M., Charlot S., Tremonti C., Brinchmann J., Bruzual G., Peng E. W., Seibert M., Bernardi M., Blanton M., Brinkmann J., Castander F., Csabai I., Fukugita M., Ivezić Z., Munn J., Nichol R., Padmanabhan N., Thakar A., Weinberg D., York D., 2003, *MNRAS*, 341, 33
- Kelson D. D., Illingworth G. D., Franx M., van Dokkum P. G., 2006, preprint, astro-ph/0606642
- Kormendy J., Djorgovski S., 1989, *ARA& A*, 27, 235
- Korn A. J., Maraston C., Thomas D., 2005, *A&A*, 438, 685
- Kroupa P., 2001, *MNRAS*, 322, 231
- Le Borgne J.-F., Bruzual G., Pelló R., Lançon A., Rocca-Volmerange B., Sanahuja B., Schaerer D., Soubiran C., Vílchez-Gómez R., 2003, *A& A*, 402, 433
- Lucia G. D., Blaizot J., 2006, preprint, astro-ph/0606519
- Maeder A., 1992, *A& A*, 264, 105
- Murphy T., 2003, PhD thesis, University of Edinburgh
- Murphy T., Meiksin A., 2004, *MNRAS*, 351, 1430
- Peebles P. J. E., 1983, *ApJ*, 274, 1
- Peebles P. J. E., Dicke R. H., 1968, *ApJ*, 154, 891
- Pickles A. J., 1985, *ApJ*, 296, 340
- Pozzetti L., Cimatti A., Zamorani G., Daddi E., Menci N., Fontana A., Renzini A., Mignoli M., Poli F., Saracco P., Broadhurst T., Cristiani S., D’Odorico S., Giallongo E., Gilmozzi R., 2003, *A&A*, 402, 837
- Roseboom I. G., et al., 2006, preprint, astro-ph/0609178
- Sawicki M. J., Lin H., Yee H. K. C., 1997, *AJ*, 113, 1
- Schlegel D. J., Finkbeiner D. P., Davis M., 1998, *ApJ*, 500, 525
- Schoenberger D., 1983, *ApJ*, 272, 708
- Stoughton C., et al. 2002, *AJ*, 123, 485
- Talbot Jr. R. J., Arnett W. D., 1971, *ApJ*, 170, 409
- Thomas D., Maraston C., Bender R., 2003, *MNRAS*, 339, 897
- Thomas D., Maraston C., Bender R., Mendes de Oliveira C., 2005, *ApJ*, 621, 673
- Trager S. C., Faber S. M., Worthey G., González J. J., 2000a, *AJ*, 120, 165
- Trager S. C., Faber S. M., Worthey G., González J. J., 2000b, *AJ*, 119, 1645
- Treu T., Stiavelli M., Casertano S., Møller P., Bertin G., 2002, *ApJ*, 564, L13
- Visvanathan N., Sandage A., 1977, *ApJ*, 216, 214
- White S. D. M., Rees M. J., 1978, *MNRAS*, 183, 341
- Worthey G., Faber S. M., Gonzalez J. J., 1992, *ApJ*, 398, 69
- Worthey G., Faber S. M., Gonzalez J. J., Burstein D., 1994, *ApJS*, 94, 687
- Worthey G., Ottaviani D. L., 1997, *ApJS*, 111, 377
- Yamada Y., Arimoto N., Vazdekis A., Peletier R. F., 2006, *ApJ*, 637, 200
- York D. G., et al. 2000, *AJ*, 120, 1579
- Yu Q., Tremaine S., 2002, *MNRAS*, 335, 965